The Plant Cell, Vol. 23: 1061–1081, March 2011, www.plantcell.org © 2011 American Society of Plant Biologists

Sphingolipids in the Root Play an Important Role in Regulating the Leaf Ionome in *Arabidopsis thaliana* [W][OA]

Dai-Yin Chao,[a,1] Kenneth Gable,[b,1] Ming Chen,[c] Ivan Baxter,[a,2] Charles R. Dietrich,[c] Edgar B. Cahoon,[c,3] Mary Lou Guerinot,[d] Brett Lahner,[a] Shiyou Lü,[a] Jonathan E. Markham,[c] Joe Morrissey,[d] Gongshe Han,[b] Sita D. Gupta,[b] Jeffrey M. Harmon,[e] Jan G. Jaworski,[c] Teresa M. Dunn,[b] and David E. Salt[a,4]

[a] Department of Horticulture and Landscape Architecture, Purdue University, West Lafayette, Indiana 47906
[b] Department of Biochemistry and Molecular Biology, Uniformed Services University of the Health Sciences, Bethesda, Maryland 20814
[c] Donald Danforth Plant Science Center, St. Louis, Missouri 63132
[d] Department of Biological Sciences, Dartmouth College, Hanover, New Hampshire 03755
[e] Department of Pharmacology, Uniformed Services University of the Health Sciences, Bethesda, Maryland 20814

Sphingolipid synthesis is initiated by condensation of Ser with palmitoyl-CoA producing 3-ketodihydrosphinganine (3-KDS), which is reduced by a 3-KDS reductase to dihydrosphinganine. Ser palmitoyltransferase is essential for plant viability. *Arabidopsis thaliana* contains two genes (At3g06060/*TSC10A* and At5g19200/*TSC10B*) encoding proteins with significant similarity to the yeast 3-KDS reductase, Tsc10p. Heterologous expression in yeast of either *Arabidopsis* gene restored 3-KDS reductase activity to the yeast *tsc10Δ* mutant, confirming both as bona fide 3-KDS reductase genes. Consistent with sphingolipids having essential functions in plants, double mutant progeny lacking both genes were not recovered from crosses of single *tsc10A* and *tsc10B* mutants. Although the 3-KDS reductase genes are functionally redundant and ubiquitously expressed in *Arabidopsis*, 3-KDS reductase activity was reduced to 10% of wild-type levels in the loss-of-function *tsc10a* mutant, leading to an altered sphingolipid profile. This perturbation of sphingolipid biosynthesis in the *Arabidopsis tsc10a* mutant leads an altered leaf ionome, including increases in Na, K, and Rb and decreases in Mg, Ca, Fe, and Mo. Reciprocal grafting revealed that these changes in the leaf ionome are driven by the root and are associated with increases in root suberin and alterations in Fe homeostasis.

INTRODUCTION

The sphingolipids are a diverse class of membrane lipids with essential functions in all eukaryotic and some prokaryotic cells. It is estimated that sphingolipids constitute up to 20 to 30% of the tonoplast and plasma membrane lipid in plants (Lynch and Dunn, 2004), and although their roles are not well defined, recent studies indicate that they have critical functions. For example, sphingolipids are reported to be enriched along with sterols in microdomains or lipid rafts (Mongrand et al., 2004; Borner et al., 2005; Sperling et al., 2005; Morel et al., 2006) that appear to selectively contain certain proteins, including several P-type H^+-ATPases, and these microdomains also mediate trafficking of plasma membrane glycosylphosphatidylinositol-anchored proteins involved in cell wall formation (Borner et al., 2005). In addition, sphingolipid metabolites, including long-chain base-1-phosphates and ceramides, have been implicated in the regulation of cellular processes such as abscisic acid–dependent guard cell closure and programmed cell death (Wang et al., 1996, 2008; Ng et al., 2001; Spassieva et al., 2002; Coursol et al., 2003, 2005; Liang et al., 2003; Townley et al., 2005; Shi et al., 2007). Here, we provide evidence that sphingolipids also play an important role in mineral ion homoeostasis.

With the exception of carbon and oxygen, plants must primarily acquire all the mineral nutrients required for growth from the soil. To achieve this, plants have evolved a complex system of specialized tissues, cellular structures, and transport molecules. This system directs the acquisition of mineral ions from the soil solution, and in certain cases, such as Fe, this also involves solubilization from the soil matrix. Soluble ions are transported across the surface of the root, in either a passive process with ions moving through the porous cell wall of the root cells or an active process with ions moving symplastically through the cells of the root. Once ions have entered the root, they can be either stored or exported to the shoot. Ion transport to the shoot usually takes place via the xylem, and plants have tight control over ions entering the shoot via the xylem through solute release and absorption by xylem parenchyma cells. Once in the leaf, ions are unloaded from the xylem and distributed throughout the leaf tissue. Ions also move via the phloem. Many steps in this complex pathway require that ions traverse various selectively permeable

[1] These authors contributed equally to this work.
[2] Current address: USDA–Agricultural Research Service Plant Genetics Research Unit, Donald Danforth Plant Science Center, 975 N. Warson Road, St. Louis, MO 63132.
[3] Current address: Center for Plant Science Innovation and Department of Biochemistry, University of Nebraska, E318 Beadle Center, 1901 Vine St., Lincoln, NE 68588.
[4] Address correspondence to dsalt@purdue.edu.
The authors responsible for distribution of materials integral to the findings presented in this article in accordance with the policy described in the Instructions for Authors (www.plantcell.org) are: Teresa M. Dunn (tdunn@usuhs.mil) and David E. Salt (dsalt@purdue.edu).
[W]Online version contains Web-only data.
[OA]Open Access articles can be viewed online without a subscription.
www.plantcell.org/cgi/doi/10.1105/tpc.110.079095

membranes, including the plasma membrane and various endomembrane systems. Such membrane transport involves ion transport proteins that are selective for specific ions, embedded within specific membranes, and are sometimes organized asymmetrical within the membrane. Furthermore, it is important that this system is regulated to integrate ion transport with both the availability of the ion in the soil and the mineral nutrient requirements of the plant as it grows and develops. Such integration is known to happen through regulation at various organizational levels, including transcriptionally and posttranslationally (for examples, see reviews by Chen et al., 2008; Maurel et al., 2009; Mikosch and Homann, 2009; Ward et al., 2009). However, many aspects of these regulatory circuits remain to be characterized. The application of high-throughput elemental profiling of mutagenized populations of *Arabidopsis thaliana*, coupled to linkage mapping, for the identification of genes involved in regulating plant mineral ion homoeostasis has been termed ionomics (Salt et al., 2008). Such an approach has been used to successfully clone genes involved in regulating the ionome (Nublat et al., 2001; Baxter et al., 2009; Tian et al., 2010), and with the development of new genomic-based tools for mapping (for example Hodges et al., 2007; Schneeberger et al., 2009), this forward genetic approach is likely to be used increasingly in the future.

Previously, we reported the identification of an *Arabidopsis* ionomic mutant with reduced leaf Ca and Mo, named *7113* (Lahner et al., 2003). Further investigations reported here revealed that this mutant has reduced leaf Mg, Ca, Fe, and Mo and elevated leaf Na, K, and Rb (a chemical analog of K) and that the mutation causing this ionomic phenotype generates a loss-of-function allele of a gene (At3g06060) that shows similarity to the yeast 3-ketodihydrosphinganine (3-KDS) reductase involved in sphingolipid biosynthesis. In both yeast and *Arabidopsis*, the enzyme serine palmitoyltransferase (SPT) is required to catalyze the condensation of Ser and palmitoyl-CoA in the first committed step in sphingolipid biosynthesis (Tamura et al., 2001; Chen et al., 2006; Dietrich et al., 2008; Teng et al., 2008). In yeast, 3-KDS reductase is then required to catalyze the NADPH-dependent reduction of 3-KDS to dihydrosphinganine (DHS) (Beeler et al., 1998). Sequence similarity searches have revealed the presence of two candidate 3-KDS reductase genes in *Arabidopsis*, At3g06060 and At5g19200. Microarray data indicated that both genes are ubiquitously expressed but that the At3g06060 gene is expressed at higher levels than the At5g19200 gene (Zimmermann et al., 2004).

Here, we report that both At3g06060 and At5g19200 genes encode functionally redundant 3-KDS reductases required for sphingolipid synthesis in *Arabidopsis*. Furthermore, our studies indicate that sphingolipids play a critical role in mineral ion homeostasis, most likely through their involvement in the ion transport functionalities of membrane systems in the root.

RESULTS

Alterations in the Leaf Ionome of *tsc10a*

The *Arabidopsis* leaf ionomic mutant *7113*, now termed *tsc10a-1*, was originally reported to have reduced leaf concentrations of Ca and Mo compared with wild-type plants (Lahner et al., 2003). Here, we extend this observation, showing that the mutant has significant ($P \leq 0.01$) increases in leaf concentrations of Na, K, and Rb and reductions in Ca, Mg, Fe, and Mo (Table 1) determined using a single-factor mixed effect model analysis of variance (ANOVA) with a Benjamini-Hochberg multiple testing correction. We further imposed the requirement that a change in concentration of an element be significant in multiple independent alleles. Using this stringent criterion, we established that three independent alleles of *tsc10a* (*tsc10a-1*, *tsc10a-2*, and *tsc10a-3*) all showed significant differences from the wild type in Na, Mg, K, Ca, Fe, Rb, and Mo ($P \leq 0.01$). We also observed that all three alleles of *tsc10a* showed reductions in both leaf concentrations of Cu and Ni but at a lower significance level ($P \leq 0.05$) (Table 1). Even though the leaf ionomes of *tsc10a-1*, *tsc10a-2*, and *tsc10a-3* are significantly altered compared with wild-type plants, we observed no major growth defects. However, in the *TSC10A* loss-of-function mutants, we do observe a reduction of root growth on media containing sucrose (see Supplemental Figure 1 online), increased frequency of tricotyledons (see Supplemental Figure 2 online), altered flower morphology (see Supplemental Figure 3A online), and reduced hypocotyl elongation in dark-grown seedlings (see Supplemental Figure 3B online).

Mapping of the Causal DNA Polymorphism in *tsc10a*

Ionomic analysis of leaf tissue sampled from F1 plants derived from the backcross Columbia-0 (Col-0) × *tsc10a-1* revealed that all 36 F1 plants showed a wild-type ionomic phenotype. These data support the conclusion that the ionomic phenotype of *tsc10a-1* is caused by a recessive mutation. Data can be found at www.ionomicshub.org in tray 1307.

To map the causal locus of *tsc10a-1*, an outcross to *Arabidopsis* Landsberg *erecta* (L*er*-0) was made and the ionomic phenotype of 277 F2 plants determined. The percentage of difference from Col-0 for leaf Mg and Ca was found to be highly correlated in the *tsc10a-1* × L*er*-0 F2 plants (correlation coefficient = 0.92), and the mutant low leaf Mg and Ca phenotype was observed in 55 of these 277 F2 plants (using a cutoff of percentage change from Col-0 wild type for Mg + Ca $\leq -20\%$), supporting our conclusion that this phenotype is caused by a single recessive locus (see Supplemental Figure 4 online). To obtain a rough map position, a bulk segregant analysis experiment (Michelmore et al., 1991) was performed with microarray detection of genetic markers (Borevitz et al., 2003; Rus et al., 2006; Baxter et al., 2008a, 2009), using the *tsc10a-1* × L*er*-0 F2 plants. Plants with the lowest leaf Mg and Ca content ($n = 31$), similar to *tsc10a-1*, and plants with Mg and Ca leaf contents similar to Col-0 ($n = 31$) were pooled separately and genomic DNA from each pool hybridized to the Affymetrix *Arabidopsis* ATH1 microarray. Using the oligonucleotide probes on the DNA microarray that show differential hybridization between L*er*-0 and Col-0 as genetic markers (single feature polymorphisms [SFPs]), the locus responsible for the leaf ionomic phenotype in *tsc10a-1* was mapped to the top 4 Mb on chromosome 3 (see Supplemental Figure 5A online). Based on this rough map position and using a combination of genotyping and confirmation

Table 1. Leaf Element Profile of Wild-Type (Col-0) and *tsc10a* Alleles

	Content (mg g^{-1} Dry Weight)				Percentage Difference from the Wild Type			
Element	Col-0	*tsc10a-1*	*tsc10a-2*	*tsc10a-3*	*tsc10a-1*	*tsc10a-2*	*tsc10a-3*	P Values
Li	24.85 ± 8.15	25.9 ± 6.66	24.69 ± 4.97	28.24 ± 6.64	4.21	−0.66	13.64	ns
B	97.32 ± 25.06	100.98 ± 64.65	83.7 ± 12.5	86.27 ± 11.44	3.76	−14	−11.36	ns
Na	**787.51 ± 157.39**	**1,038.65 ± 207.57**	**1,009.35 ± 151.24**	**1,004.75 ± 201.80**	**31.89**	**28.17**	**27.59**	**0.01**
Mg	**8,712.78 ± 444.89**	**6,958.47 ± 668.67**	**6929 ± 318.53**	**7,058.04 ± 640.89**	**−20.13**	**−20.47**	**−18.99**	**<0.0003**
P	7,255.06 ± 884.98	7,087.65 ± 747.33	7,144.37 ± 502.22	7,335.26 ± 663.50	−2.31	−1.53	1.11	ns
S	4,373.87 ± 1,606.38	5,083.81 ± 1,749.13	5,216.61 ± 952.92	5,678.65 ± 1,453.15	16.23	19.27	29.83	ns
K	**38,027.81 ± 4,819.13**	**47,103.09 ± 4,906.54**	**48,937.27 ± 2,451.13**	**47,437.71 ± 3,886.14**	**23.86**	**28.69**	**24.74**	**<0.0003**
Ca	**53,702.58 ± 4,237.14**	**42,409.7 ± 5,209.34**	**41,416.67 ± 3,316.2**	**42,553.35 ± 4,329.93**	**−21.03**	**−22.88**	**−20.76**	**<0.0003**
Mn	79.79 ± 44.33	61.16 ± 13.13	57.13 ± 13.72	61.99 ± 10.53	−23.34	−28.4	−22.30	ns
Fe	**129.64 ± 8.89**	**105.66 ± 10.31**	**102.2 ± 7.15**	**106.17 ± 8.92**	**−18.5**	**−21.17**	**−18.1**	**<0.0003**
Co	0.39 ± 0.15	0.57 ± 0.23	0.53 ± 0.19	0.63 ± 0.22	47.66	36.96	63.43	ns
Ni	11.76 ± 70	7.8 ± 10	7.64 ± 0.53	8.13 ± 0.88	−33.65	−35.04	−30.81	0.04
Cu	7.65 ± 5.33	4.17 ± 0.9	4.85 ± 0.63	4.86 ± 0.79	−45.48	−36.59	−36.42	0.03
Zn	116.12 ± 29.01	114.88 ± 28.94	121.26 ± 53.54	107.18 ± 19	−1.07	4.43	−7.70	ns
As	0.19 ± 0.07	0.27 ± 0.09	0.27 ± 0.13	0.37 ± 0.28	37.32	36.84	89.18	ns
Se	8.22 ± 2.98	11.6 ± 3.98	10.96 ± 3.62	13.4 ± 3.54	41.13	33.3	62.93	nsf
Rb	**35.85 ± 4.34**	**44.88 ± 4.64**	**46.93 ± 4.23**	**47.5 ± 4.46**	**25.2**	**30.89**	**32.51**	**<0.0003**
Mo	**8.63 ± 2.77**	**3.15 ± 1.63**	**2.69 ± 0.65**	**2.6 ± 0.50**	**−63.46**	**−68.77**	**−69.90**	**<0.0003***
Cd	1.18 ± 0.27	1.38 ± 0.44	1.1 ± 0.34	1.43 ± 0.41	17.51	−6.23	21.23	ns

Data represent the mean of 12 independent plants per genotype ± SD. Data in bold represent elements with significant difference ($P \leq 0.01$) between the mutant and the wild type in all three independent alleles. The raw elemental concentrations for individual plant samples are available at www.ionomicshub.org in experimental tray 1458. ns, not significant; nsf = not significant due to failure to meet requirement that all alleles are significantly different from the wild type; asterisk, square root transformed after significant Levene's homogeneity of variance test.

of the leaf ionomic phenotype in the F3 generation, we were able to initially map the causal mutation to a region of 400 kb between simple sequence length polymorphic (SSLP) markers T1540k and T1.9M using 341 (*tsc10a-1* × L*er*-0) F2 plants (see Supplemental Figure 5B online). Fine mapping within this region using 1279 (*tsc10a-1* × Ler-0) F2 plants narrowed down the location of the causal mutation in *tsc10a-1* to a 30-kb interval between markers T1818K and T1848K (see Supplemental Figure 5C online). DNA sequencing of this 30-kb region revealed a G-to-T single nucleotide polymorphism in *tsc10a-1* that generates a premature translational stop codon in the first exon of the At3g06060 gene, 161 amino acids earlier than in wild-type Col-0 (see Supplemental Figure 5D online).

To establish that loss of function of At3g06060 is driving the leaf ionomic phenotype observed in *tsc10a-1*, we obtained two T-DNA insertional alleles, SALK_149589 and SAIL_131_A01, which were named *tsc10a-2* and *tsc10a-3*, respectively. The insertion site of SALK_149589 was confirmed to be in exon 1, in the same orientation as the gene, and to be located 66 bp downstream from the start codon of At3g06060 (see Supplemental Figure 5D online). The insertion in the SAIL_131_A01 line was in the third exon, 1605 bp downstream of the start codon of At3g06060 (see Supplemental Figure 5D online). Ionomic analysis of leaf tissue of the *tsc10a-2* and *tsc10a-3* mutants confirmed that they have the same leaf ionomic phenotype as *tsc10a-1* (Table 1, Figure 1A). Furthermore, transformation of *tsc10a-1* with a genomic DNA fragment containing the wild-type At3g06060 gene and a 1.2-kb upstream region containing the native promoter fully complements the mutant leaf ionomic phenotype of *tsc10a-1* back to the wild type in three independently transformed lines (Figure 1B). Furthermore, quantitative RT-PCR (qRT-PCR) confirmed that expression of the At3g06060 gene is reduced in *tsc10a-1* consistent with the occurrence of nonsense-mediated mRNA decay and also in both the T-DNA insertional alleles *tsc10a-2* and *tsc10a-3* (Figure 2A). Taken together, this evidence establishes that loss of function of At3g06060 is driving the observed leaf ionomic phenotype.

Sequence similarity searches using the predicted amino acid sequence of At3g06060 as the query identified the yeast 3-KDS reductase (temperature-sensitive Csg2 suppressor protein [Tsc10p]) (see Supplemental Figure 6A online), and based on this homology, we named the At3g06060 gene *TSC10A*. Although sequence similarity of the encoded TSC10A protein to yeast Tsc10p is low, being ~18% identical and 40% similar, the sequence similarity extends over the length of the proteins and includes critical residues that identify them as members of the family of enzymes known as the short-chain reductases (SDRs) (Kavanagh et al., 2008). While there are many predicted SDRs in *Arabidopsis*, the remaining members of the family have more limited similarity to Tsc10p. Moreover, the protein encoded by At3g06060 has higher sequence similarity to the mammalian 3-KDS reductase FVT1 (32% identity; 55% similarity) than to Tsc10p (see Supplemental Figure 6A online).

Analysis of the *Arabidopsis* genome revealed a second gene, At5g19200, on chromosome 5 with a similarity of 86.5% to the predicted amino acid sequence of *TSC10A* (see Supplemental

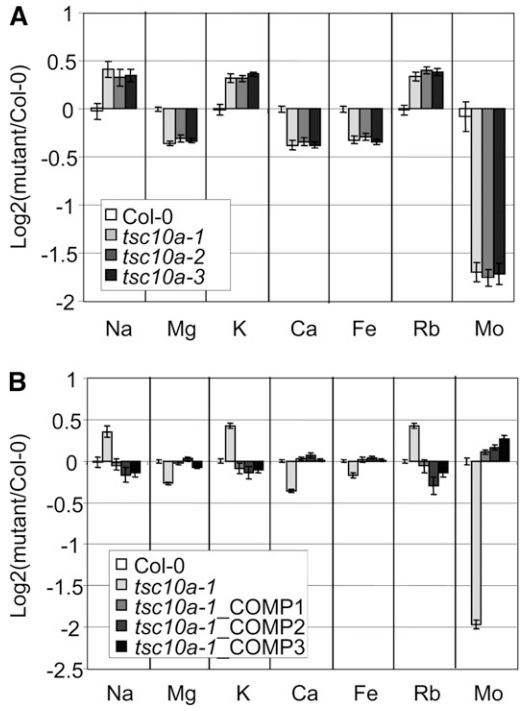

Figure 1. Loss of Function of *TSC10a* Confers Changes in the Leaf Ionome in *Arabidopsis*.

(A) Comparison of the leaf ionome of various *tsc10a* alleles.
(B) Comparison of the leaf ionome of *tsc10a-1* and after complementation with the wild-type gene (*tsc10-1*_COMP).
For each element in **(A)** and **(B)**, the mean concentration of the element in wild-type Col-0 was used as the reference, and the log2 of the ratio of each mutant divided by the reference was calculated. Data represent means ± SE of 12 independent replicate plants per genotype. Data for **(A)** are derived from the same experiment as described in Table 1. Raw data for **(B)** can be obtained from www.ionomicshub.org in tray 1531.

Figure 6A online). Based on its similarity to *TSC10A*, At5g19200 was named *TSC10B*. Two T-DNA insertional alleles of *TSC10B* were obtained (SAIL_659_C12 and GABI_524F10). The T-DNA insertion for SAIL_659_C12 was verified to reside 894 bp downstream of the start codon within the first intron and in the reverse orientation relative to the *TSC10B* gene (see Supplemental Figure 6B online), and this T-DNA allele was named *tsc10b-1*. The T-DNA insertional for GABI_523F10 was verified to be inserted in the second intron, and this T-DNA allele was named *tsc10b-2*. qRT-PCR confirmed that *TSC10B* expression is significantly reduced in both *tsc10b-1* and *tsc10b-2* (Figure 2B). Interestingly, qRT-PCR analysis of the steady state levels of *TSC10A* mRNA in the *tsc10b-1* and *tsc10b-2* mutants revealed that loss of expression of *TSC10B* is compensated for by a concomitant increase in the expression of *TSC10A* in both shoots and roots of *tsc10b-1* and *tsc10b-2* (Figure 2B).

Analysis of the leaf ionome of two alleles of *tsc10b* (*tsc10b-1* and *tsc10b-2*) revealed significant alterations compared with the wild type, determined using a single-factor mixed effect model ANOVA with a Benjamini-Hochberg multiple testing correction. We further imposed the requirement that a change in concentration of an element be significant in multiple independent alleles. Using this stringent criterion, we established that both independent alleles of *tsc10b* (*tsc10b-1* and *tsc10b-2*) showed significant differences from the wild type in Li, B, K, Ca, Fe, Rb, Mo, and Cd ($P \leq 0.01$) (Table 2).

Loss of Function of Both *TSC10A* and *TSC10B* Is Lethal in *Arabidopsis*

When grown in standard growth chamber conditions, plants with disruption of either *TSC10A* or *TSC10B* have no major growth phenotype. Because 3-KDS reductase activity is expected to be required for synthesis of sphingolipids, known to be essential for plant viability (Chen et al., 2006; Dietrich et al., 2008), this presumably reflects functional redundancy of the two putative 3-KDS reductases. This was examined further by generation of double mutants for the two 3-KDS genes. For these studies, crosses were made between *tsc10a-2* and *tsc10b-2* mutants as well as *tsc10a-3* and *tsc10b-2* mutants to generate F1 plants. PCR genotyping of 96 plants from the segregated F2 population obtained from selfing of F1 plants from the *tsc10a-1* × *tsc10b-2* cross did not reveal any homozygous double mutant plants. To further establish that the double mutants were not viable, an additional 96 plants were genotyped from the progeny of the *tsc10a-1/tsc10a-2 tsc10b-2*/+ selfed plants. If the two 3-KDS genes were not essential, one-quarter of this population would be expected to be homozygous for knockout of both genes. Instead, no homozygous double mutants were obtained, indicating that the 3-KDS genes encode an essential activity in *Arabidopsis*. Consistent with this, no double mutant progeny were recovered among 160 genotyped plants from a segregating F2 population from a *tsc10a-3* × *tsc10b-2* cross. To unequivocally establish that the two 3-KDS genes are essential, genetic complementation studies were conducted. For these experiments, *tsc10a-2/tsc10a-2 tsc10b-2*/+ plants were transformed with a construct carrying a wild-type copy of the *TSC10A* gene. While no homozygous double mutants were confirmed in the T1 plants, plants disrupted in both genes but carrying the transgenic genomic *TSC10A* gene in the T2 plants were recovered (data not shown). Overall, these results indicate that *TSC10A* and *TSC10B* are functionally redundant genes, but mutation of both genes results in loss of viability. The latter finding is consistent with results from yeast that have established that 3-KDS reductase catalyzes an essential activity (Beeler et al., 1998).

TSC10A and *TSC10B* in *Arabidopsis* Are Expressed throughout the Plant

To help understand how loss of function of *TSC10A* could cause the observed leaf ionomic phenotype, we examined tissue expression patterns of both *TSC10A* and *TSC10B* using qRT-PCR. We observed that both genes are expressed in seedlings and in root, leaf, stem, flower, and developing siliques (Figure 3), with *TSC10A* being expressed more highly than *TSC10B* in all tissues in which it was measured. Furthermore, microarray data support this plant-wide expression of both genes (Zimmermann et al., 2004).

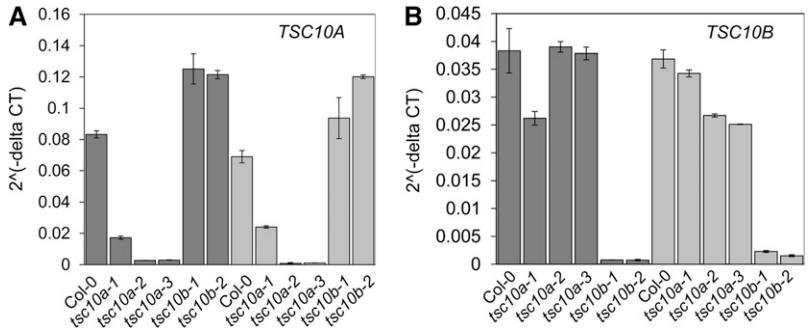

Figure 2. Interrelationship of Expression Patterns of *Arabidopsis TSC10A* and *TSC10B*.

qRT-PCR analysis of expression of *TSC10A* **(A)** and *TSC10B* **(B)** in shoot (dark-gray bars) and root (light-gray bars) of Col-0 and various alleles of the *tsc10a* and *tsc10b* mutants. *Ubc* (for *Ubiquitin C*) was used as the control gene, and four PCR reactions were done per replicate using three independent biological samples per genotype, with error bars representing SD.

The *Arabidopsis TSC10A* and *TSC10B* Genes Substitute for Yeast *TSC10*

The candidate 3-KDS reductases from *Arabidopsis* (TSC10A and TSC10B) were initially tested for function by determining whether their expression reversed the phenotypes associated with yeast *tsc10* mutants. For these functional complementation studies, cDNA fragments encoding the full-length *Arabidopsis* proteins were PCR amplified and inserted into the yeast pADH plasmid for constitutive expression with an N-terminal hemagglutinin (HA) tag. The yeast *tsc10-1* mutant with a temperature-sensitive mutation in the essential *TSC10* gene (Beeler et al., 1998; Dunn et al., 2000) and the *tsc10Δ* mutant were used for the functional complementation studies. Both strains have defects in 3-KDS reductase required for catalysis of the reduction of 3-KDS to dihydrosphingosine, the second step in sphingolipid biosynthesis (Figure 4A). Expression of either *TSC10A* or *TSC10B* from *Arabidopsis* restored growth to the yeast *tsc10-1* mutant at the restrictive temperature (Figure 4B). Although the *tsc10Δ* mutation is lethal, the null mutants can be rescued by chemical complementation with long-chain bases (LCBs), such as phytosphingosine (PHS). Expression of either *TSC10A* or *TSC10B* from *Arabidopsis* also reversed the LCB requirement of the *tsc10Δ* mutant cells (Figure 4B). We previously reported that the

Table 2. Leaf Element Profile of Wild-Type (Col-0) and *tsc10b* Alleles

	Content (mg g^{-1} Dry Weight)			Percentage Difference from the Wild Type		
Element	Col-0	*tsc10b-1*	*tsc10b-2*	*tsc10b-1*	*tsc10b-2*	P Values
Li	**8.94 ± 2.93**	**13.07 ± 3.98**	**14.81 ± 3.68**	**46.15**	**65.60**	**0.0025**
B	**137.96 ± 21.73**	**107.72 ± 12.34**	**99.72 ± 8.06**	**−21.92**	**−27.72**	**<0.0004***
Na	704.14 ± 96.74	852.79 ± 175.00	839.96 ± 97.22	21.11	19.29	0.02
Mg	6,678.70 ± 306.29	6,729.38 ± 299.69	6,779.26 ± 452.37	0.76	1.51	ns
P	7,459.84 ± 706.62	6,622.51 ± 707.24	6,671.09 ± 844.73	−11.22	−10.57	0.03
S	7,442.30 ± 884.48	7,519.10 ± 789.05	7,911.46 ± 989.18	1.03	6.30	ns
K	**40,998.90 ± 4,130.59**	**26,096.86 ± 3,457.08**	**28,343.63 ± 4,878.71**	**−36.35**	**−30.87**	**<0.0004**
Ca	**24,511.29 ± 1,801.65**	**28,938.80 ± 1,769.44**	**28,253.75 ± 2,396.99**	**18.06**	**15.27**	**<0.0004**
Mn	78.40 ± 29.60	75.71 ± 31.23	62.41 ± 15.62	−3.43	−20.40	ns
Fe	**75.69 ± 3.31**	**71.52 ± 3.75**	**71.72 ± 2.72**	**−5.51**	**−5.25**	**0.01**
Co	0.54 ± 0.08	0.49 ± 0.06	0.47 ± 0.06	−8.85	−12.63	ns
Ni	0.39 ± 0.10	0.42 ± 0.05	0.42 ± 0.05	7.63	7.49	ns
Cu	6.73 ± 1.02	6.03 ± 0.71	6.00 ± 0.56	−10.37	−10.90	ns
Zn	73.08 ± 10.77	81.86 ± 9.43	75.01 ± 5.78	12.02	2.65	ns
As	0.94 ± 0.34	0.67 ± 0.18	0.70 ± 0.21	−28.39	−25.92	0.04
Se	3.47 ± 1.70	3.83 ± 0.96	5.18 ± 1.23	10.48	49.47	0.02
Rb	**62.18 ± 12.63**	**41.34 ± 6.68**	**45.92 ± 9.01**	**−33.52**	**−26.14**	**<0.0004**
Mo	**12.05 ± 2.36**	**19.59 ± 3.16**	**19.27 ± 3.46**	**62.57**	**59.85**	**<0.0004**
Cd	**0.55 ± 0.08**	**0.68 ± 0.05**	**0.66 ± 0.08**	**23.34**	**20.31**	**0.0006**

Data represent the mean of 12 independent plants per genotype ± SD. Data in bold represent elements with a significant difference ($P \leq 0.01$) between the mutant and the wild type in both independent alleles. The raw elemental concentrations for individual plant samples are available at www.ionomicshub.org in experimental tray 1860. ns, not significant; asterisk, inverse transformed after significant Levene's homogeneity of variance test.

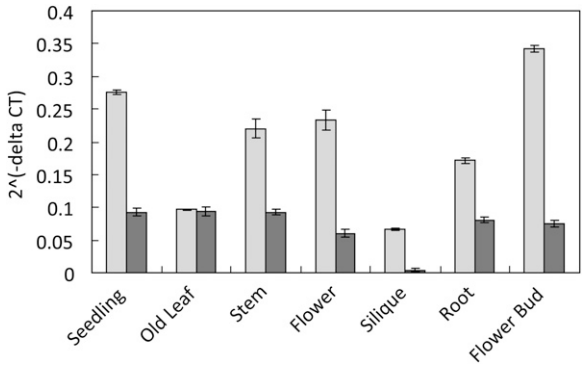

Figure 3. Expression Pattern of *TSC10A* and *TSC10OB* in *Arabidopsis*.

qRT-PCR analysis of *TSC10A* (light-gray bars) and *TSC10B* (dark-gray bars) expression in various tissues of wild-type *Arabidopsis* plants (Col-0). *Ubc* was used as the control gene, and four PCR reactions were done per replicate using three independent biological samples per genotype, with error bars representing SD.

yeast *tsc10-1* mutant, deficient in 3-KDS reductase, accumulates 3-KDS, an intermediate that is not detected in wild-type yeast (Figure 4C). Here, we observe that expression of either *TSC10A* or *TSC10B* from *Arabidopsis* reduced this accumulation of 3-KDS in the yeast *tsc10-1* mutant (Figure 4C), providing additional evidence that both *TSC10A* and *TSC10B* from *Arabidopsis* encode functional 3-KDS reductases.

3-KDS Reductase Assays Reveal That TSC10A from *Arabidopsis* Lacks Stereospecificity

To further characterize the *Arabidopsis* TSC10 proteins, their in vitro 3-KDS reductase activities were investigated. For these experiments [^{14}C]-3-KDS was prepared using a purified bacterial SPT enzyme from *Sphingomonas paucimobilis*. Unlike the eukaryotic SPT enzymes, bacterial SPT is a soluble homodimeric enzyme that can be used to generate large quantities of [^{14}C]-3-KDS for use in the 3-KDS reductase assay (Gupta et al., 2009). Purified [^{14}C]-3-KDS was added to microsomes prepared from yeast *tsc10Δ* mutant cells expressing the yeast HA-tagged-Tsc10p, or the *Arabidopsis HA-TSC10A* or *HA-TSC10B* and its conversion to [^{14}C]-DHS was measured. Microsomes prepared from yeast expressing the yeast HA-Tsc10p or the *Arabidopsis HA-TSC10A* or *HA-TSC10B* all contained HA-tagged proteins of the predicted molecular mass (~40 kD) detected by immunobolting using anti-HA antibodies (Figure 5A). Microsomes prepared from *tsc10Δ* mutant cells harboring the empty pADH1 vector displayed no 3-KDS reductase activity, whereas those expressing the yeast Tsc10p and the *Arabidopsis TSC10A* or *TSC10B* showed an NADPH-dependent conversion of [^{14}C]-3-KDS to [^{14}C]-DHS (Figure 5B). Because each of the proteins was HA tagged, it was possible to estimate the abundance of each 3-KDS reductase by comparison to purified HA-tagged bacterial SPT (Figure 5A) and thus to estimate the specific activities of the yeast and *Arabidopsis* enzymes. From these analyses, we concluded that the yeast Tsc10p has a specific activity of ~30 μmol mg^{-1} min^{-1} and the *Arabidopsis* TSC10A of ~85 μmol mg^{-1} min^{-1} and TSC10B of ~500 μmol mg^{-1} min^{-1}. Both of the *Arabidopsis* 3-KDS reductases displayed higher activities with NADPH as cofactor, but in contrast with yeast Tsc10p, also used NADH (Figures 5C and 5D). To assess substrate specificity, [^{14}C]-3-KDS with different chain lengths was prepared by incubating the bacterial SPT with [^{14}C]-Ser and acyl-CoAs of different chain lengths. Only the reduction of C18-[^{14}C]-3-KDS and C20-[^{14}C]-3-KDS by the *Arabidopsis* enzymes is shown in Figure 5C, but all three enzymes efficiently reduced 3-KDSs with chain lengths from C12 to C20.

Thin layer chromatograms of the products of the enzyme assays revealed that the *Arabidopsis* TSC10A catalyzed the conversion of 3-KDS to two products (note the doublet in Figure 5C) when NADPH was used as cofactor. This suggested that the *Arabidopsis* TSC10A enzyme transferred the hydride from NADPH to either face of the ketone substrate, thereby forming both D-erythro and L-threo DHS. Consistent with this hypothesis, chemical reduction of 3-KDS with sodium borohydride ($NaBH_4$) produced products with the same mobilities as those formed by TSC10A (Figure 5C). By contrast, the *Arabidopsis* TSC10B and the yeast Tsc10p appear to be more stereoselective, yielding a single DHS product. To directly investigate whether the *Arabidopsis* TSC10A produced both stereoisomers, the products of the reactions were extracted, derivatized with AccQ, and analyzed along with commercially available standards by HPLC. As shown in Figure 5E, the two products formed by the *Arabidopsis* TSC10A did indeed coelute with the L-threo and D-erythro standards and with the products produced by chemical reduction of 3-KDS with $NaBH_4$. We therefore conclude that the *Arabidopsis* TSC10A enzyme produced both the physiologically relevant D-erythro DHS, as well as L-threo DHS, also known as safingol, a compound that is in clinical trials as a potential anticancer drug (Morales et al., 2007).

The *Arabidopsis* 3-KDS Reductases Are Localized to the Endoplasmic Reticulum and Have an N-Terminal Membrane-Spanning Domain That Is Not Present in Yeast Tsc10p

To understand further the function of the *Arabidopsis* TSC10 proteins, we examined their subcellular localization. We prepared a cDNA construct that when translated would generate a chimeric protein with the green fluorescent protein (GFP) fused to the N terminus of TSC10A (GFP-TSC10A) and TSC10B (GFP-TSC10B). Protoplasts isolated from tobacco (*Nicotiana tabacum*) BY-2 cells were cotransformed with *GFP-TSC10A* or *GFP-TSC10B* and the endoplasmic reticulum (ER) marker *CD3-959* (Nelson et al., 2007) fused with the red fluorescent protein (*mCherry*), and in these cells both green and red fluorescence was observed to colocalize (Figures 6A and 6B). Such colocalization of green fluorescence from GFP-TSC10A and GFP-TSC10B with the red fluorescence from the bona fide ER marker CD3-959 confirms the ER localization of both the TSC10A and TSC10B proteins. Expression of *GFP-TSC10A* was also found to complement the leaf ionomic phenotype of *tsc10a-1*, supporting the conclusion that the observed ER localization of the TSC10 proteins is functional.

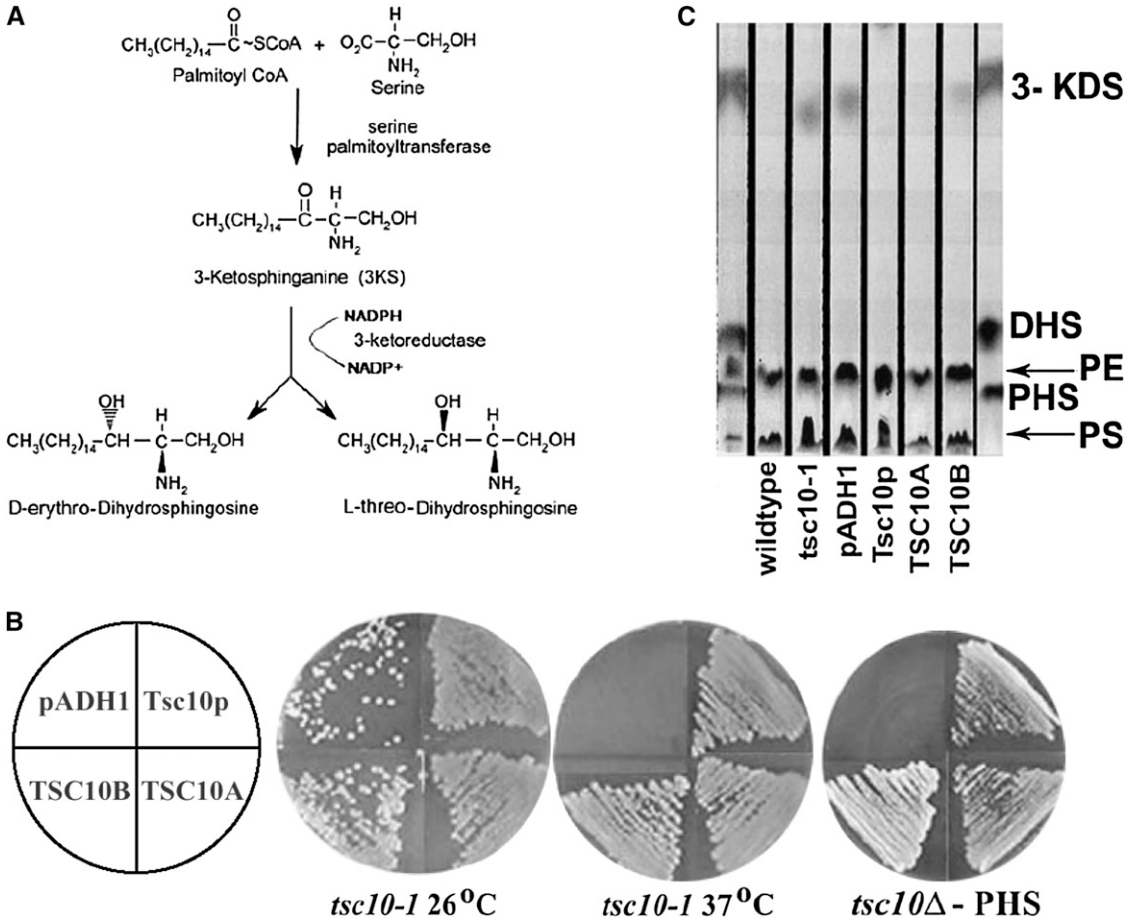

Figure 4. Both TSC10A and TSC10B Function as 3-Ketosphinganine Reductases.

(A) Pathway for sphingolipid biosynthesis in plants.

(B) Yeast functional complementation. Expression of yeast TSC10 and *Arabidopsis* TSC10A or TSC10B reverses the temperature-sensitive phenotype of the yeast *tsc10-1* mutant and the LCB requirement of the yeast *tsc10Δ* mutant.

(C) The yeast *tsc10-1* mutant cells accumulate 3-KDS. The empty expression vector (pADH1) does not alter this phenotype, but plasmids expressing yeast *TSC10* or either *Arabidopsis TSC10* gene reverse the accumulation of 3-KDS. The PHS, DHS, and 3-KDS standards (outside lanes) migrated to the indicated positions. DHS R_F value = 0.3 and 3-KDS R_F value = 0.7. Phosphatidylserine and phosphatidylethanolamine, coextracted with the LCBs, also stain with ninhydrin.

Both Tsc10p from yeast and TSC10A and TSC10B from *Arabidopsis* are localized at the ER, catalyze the same reaction, and have the conserved predicted catalytic residues (see Supplemental Figure 6A online) that are expected to lie on the cytoplasmic face of the ER membrane. In addition, these proteins have two potential transmembrane domains (TMDs) near their C termini. However, both the *Arabidopsis* TSC10A and TSC10B enzymes have different predicted membrane topologies compared with the yeast Tsc10p. In particular, the *Arabidopsis* 3-KDS reductases have a hydrophobic N-terminal extension that is predicted to contain an additional TMD that would place the N termini of the *Arabidopsis* proteins in the ER lumen (see Supplemental Figure 6A online). To experimentally address this, glycosylation reporter cassettes (GC) were inserted at the N and C termini of the yeast Tsc10p and the *Arabidopsis* TSC10A. Each cassette consisted of a 53–amino acid domain comprising residues 80 to 133 of yeast invertase (Suc2p) that contains three NXS/T sites for N-linked glycosylation (Nakajima et al., 1994). In the case of Tsc10p, no glycosylation was observed on either the N- or C-terminally located GC cassette (Figure 6C), suggesting that the protein has an even number of membrane-spanning domains. Several algorithms predict the presence of two TMDs located between 255 to 275 and 285 to 305, and in each case, they also predict a third TMD at 160 to 180. However, since this region contains the predicted catalytic residues (see Supplemental Figure 6A online) that are characteristic of the SDRs, it is not likely to be in the membrane. In addition, the presence of three TMDs is inconsistent with the glycosylation data, making it likely that the two predicted membrane spanning domains in the C-terminal region of the yeast Tsc10p tether the protein to the membrane with both ends located in the cytoplasm. In contrast with the cytoplasmic

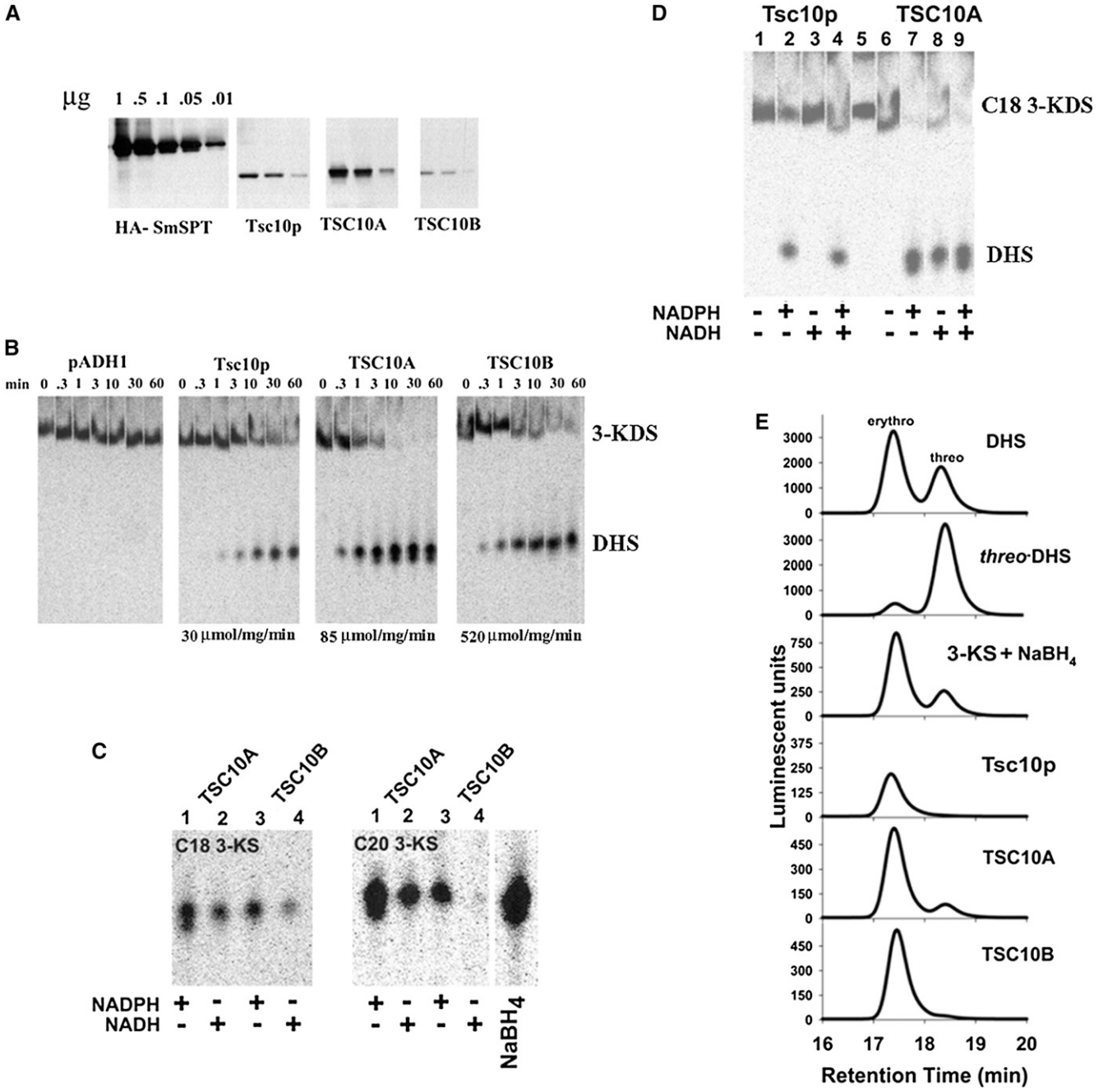

Figure 5. Enzymological Analysis of *Arabidopsis* TSC10.

(A) Microsomal protein (10, 5, or 1 μg) preparations from *tsc10Δ* mutants expressing *HA-Tsc10p*, *HA-TSC10A*, or *HA-TSC10B*. The proteins were resolved by SDS-PAGE and determined by immunoblotting using HA antibody. The purified HA-tagged bacterial SPT protein (HA-SmSPT) was used as a control.

(B) In vitro activities of *Arabidopsis* TSC10 and yeast TSC10. Microsomal proteins (40 μg) from **(A)** were added to a reaction mix containing NADPH and ^{14}C-3-KDS. At the indicated times, aliquots were removed and the LCBs extracted and resolved by thin layer chromatography. The amount of DHS formed was quantitated by phosphorimaging and specific activities calculated. DHS R_F value = 0.3 and 3-KDS R_F value = 0.7.

(C) and **(D)** The dependency of *Arabidopsis* TSC10 and yeast TSC10 activity on NADPH. Sodium borohydride ($NaBH_4$) was used as a positive control. DHS R_F value = 0.3 and 3-KDS R_F value = 0.7.

(E) Stereospecificity of *Arabidopsis* TSC10. LCBs were extracted following reduction of 3-KDS with Tsc10p, TSC10A, or TSC10B, derivatized with AccQ, and analyzed by HPLC. As controls, a mixture of L-threo- and D-erythro-DHS, L-threo-DHS, and $NaBH_4$-reduced 3-KDS were also AccQ derivatized for HPLC analysis.

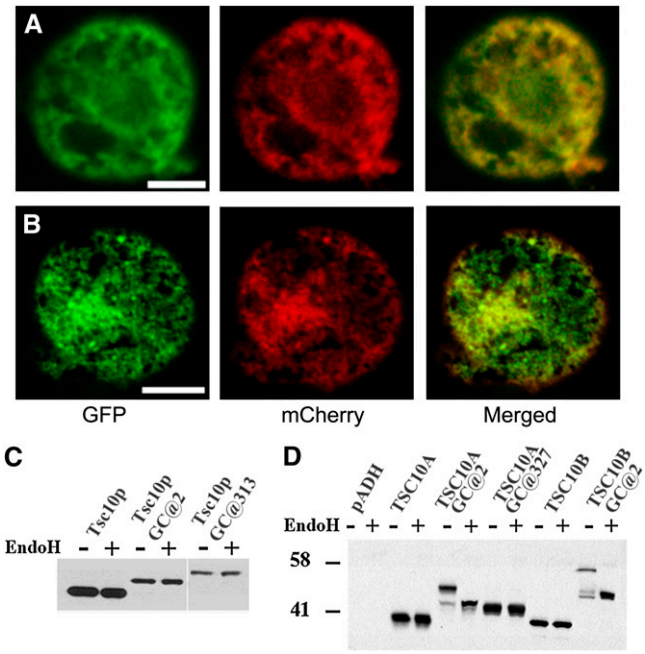

Figure 6. Subcellular Distribution and Membrane Topologies of *Arabidopsis* TSC10.

TSC10A and TSC10B were localized on the ER membrane as determined by cotransient expression of *GFP-TSC10A* **(A)** or *GFP-TSC10B* **(B)** with the ER marker *CD3-959-mCherry*. Transient expression was performed in protoplasts of tobacco BY-2 cells. The membrane topologies of *Arabidopsis* TSC10A and TSC10B are different from yeast Tsc10p. Both the N and C termini of yeast Tsc10p are cytoplasmic **(C)**, while N termini of *Arabidopsis* TSC10A and TSC10B are luminal **(D)**. A GC was inserted in-frame into yeast Tsc10p and *Arabidopsis* TSC10A and TSC10B after the initiator Met (GC@2) or before the stop codon of Tsc10p (GC@313) or TSC10A (GC@327), and the fusion proteins were expressed in *tsc10Δ* yeast mutant cells. The glycosylation status of the proteins was assessed by incubating microsomal protein with or without endoH and analyzing 15 μg by immunoblotting using anti-HA antibodies.

localization of the N terminus of the yeast Tsc10p, the N terminus of *Arabidopsis* TSC10A is clearly lumenal since the GC cassette inserted after codon 2 was glycosylated. As shown in Figure 6D, treatment of solubilized membranes with EndoH increased the electrophoretic mobility of TSC10AGC@2. Similar to yeast Tsc10p, the C terminus of the *Arabidopsis* TSC10A is apparently cytoplasmic since the electrophoretic mobility of TSC10AGC@327, with a GC cassette at its C terminus, was not affected by EndoH (Figure 6D). The GC cassette at the N terminus of *Arabidopsis* TSC10B was also glycosylated (Figure 6D), and although we did not experimentally demonstrate that the C terminus of TSC10B is cytoplasmic, we presume that both proteins are oriented with their N termini in the lumen and their C termini in the cytoplasm. These results imply the presence of an additional membrane-spanning domain in the N-terminal extension of the *Arabidopsis* proteins (see Supplemental Figure 6A online). Thus, while the C-terminal regions of the *Arabidopsis* TSC10A and TSC10B are topologically similar to the yeast Tsc10p, the N-terminal regions of the *Arabidopsis* proteins are clearly distinct from the yeast protein.

3-KDS Reductase Activity and Sphingolipid Biosynthesis Are Perturbed in the *tsc10 Arabidopsis* Mutants

To verify the function of TSC10A and TSC10B in *Arabidopsis*, we measured the 3-KDS reductase activities in *tsc10a-2* and *tsc10b-2* compared with wild-type plants. Microsomes were prepared from whole-plant extracts of 8-week-old plants grown under short-day conditions and 3-KDS reductase activity determined by measuring the conversion of [^{3}H]-3-KDS to [^{3}H]-DHS. Microsomal membranes prepared from *tsc10a-2* mutant plants lacking expression of *TSC10A* showed virtually no NADPH-dependent 3-KDS reductase activity, compared with wild-type plants (Figure 7), indicating that the *TSC10A* gene encodes the majority of all the 3-KDS reductase activity in *Arabidopsis*. Interestingly, microsomal membranes prepared from *tsc10b-2* mutant plants lacking expression of *TSC10B* showed elevated 3-KDS reductase activity compared with wild-type plants (Figure 7). Elevated 3-KDS reductase activity in *tsc10b-2* is consistent with both the elevated level of *TSC10A* expression observed in this mutant (Figure 2A) and its leaf ionomic phenotype, which is opposite to *tsc10a* (Table 2).

To further investigate the effect of loss of 3-KDS reductase activity on sphingolipid biosynthesis, we performed profiling of the sphingolipid content of 7-d-old seedlings of wild-type (Col-0), *tsc10a-2*, and *tsc10b-2* mutants grown under light and dark conditions. The rational for choosing these experimental conditions is that *tsc10a-2* displays reduced hypocotyl elongation compared with the wild type under these conditions (see Supplemental Figure 3B online), suggesting that the defect in sphingolipid biochemistry may be most pronounced under these growth conditions. As expected, 3-KDS reductase-deficient plants showed an accumulation of a small amount of 3-KDS (Figure 8A), which was largely converted to 4-hydroxy-3-KDS, presumably through the action of sphingoid base hydroxylase. Despite the reduction in 3-KDS reductase activity, free

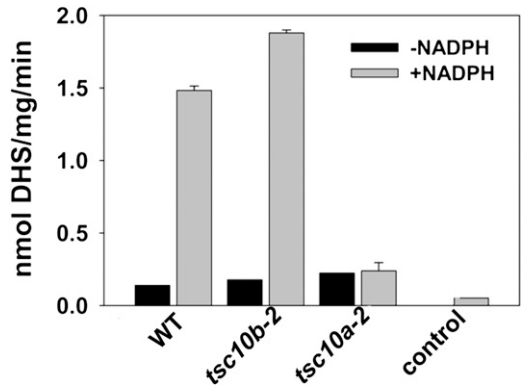

Figure 7. 3-KS Reductase Activity in the *Arabidopsis* Mutants *tsc10a* and *tsc10b* and Wild-Type Col-0.

Microsomes were prepared from the wild type (WT), *tsc10a-2*, and *tsc10b-2* and NADPH-dependent 3-KDS reductase activities measured. For assays done in the presence of NADPH, data represent means (n = 3) ± SD. Assays done in the absence of NADPH were performed at n = 1.

phytosphingosine (t18:0) and phytosphingosine-1-phosphate (t18:0-P) were accumulated to higher levels than wild-type plants grown under the same conditions (Figure 8A). Analysis of the complex sphingolipid content (Figure 8B) showed that free ceramide and hydroxyceramide accumulated to higher levels in *tsc10a-2* than in wild-type plants at the cost of glucosylceramide (GlcCer), suggesting a specific block in GlcCer synthesis as the level of glycosyl inositolphosphoceramide was unaffected. The mechanism by which decreased 3-KDS reductase activity leads to inhibition of GlcCer synthesis is not known but may be a result of pathway inhibition by the accumulated (4-hydroxy)-3-KDS or an acylated derivative thereof. These data point to a significant alteration of sphingolipid metabolism in tissues of the *tsc10a-2* mutant.

Reduced 3-KDS Reductase Activity in *Arabidopsis* Roots Drives Changes in the Leaf Ionome

TSC10A in *Arabidopsis* is expressed in both roots and shoots (Figures 2A and 3). To determine in which tissue loss of 3-KDS

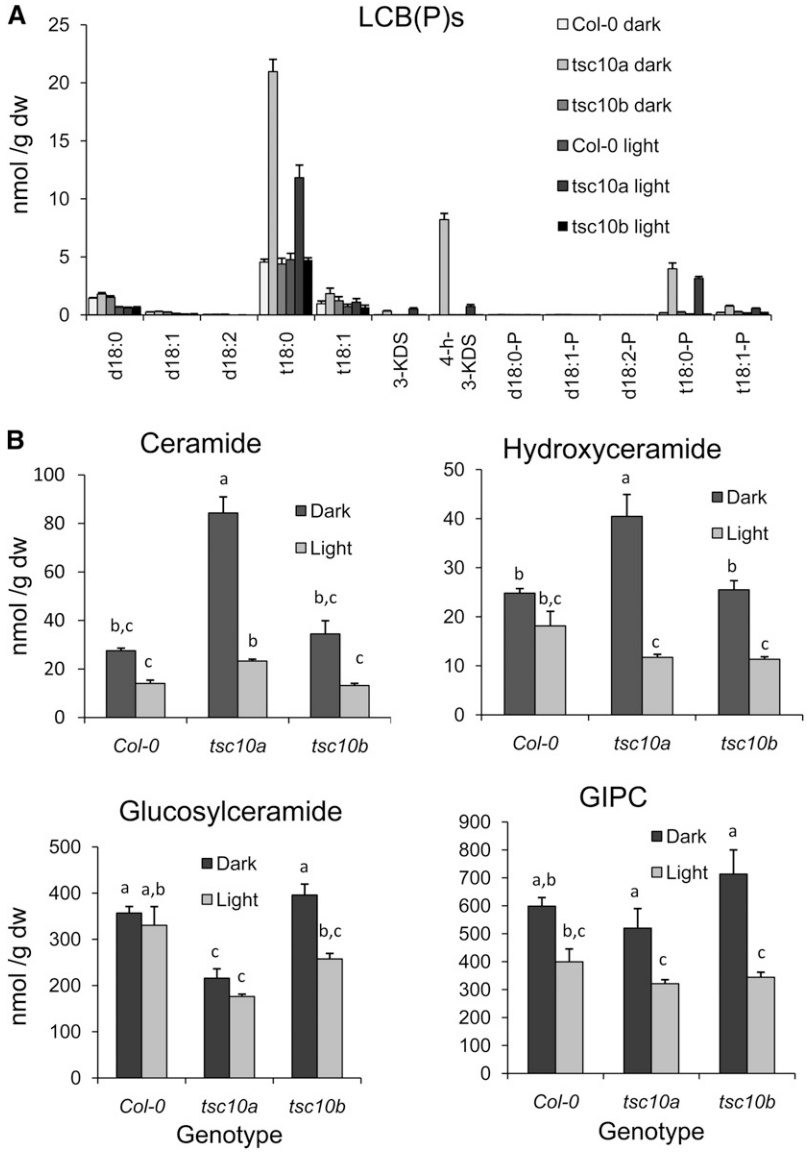

Figure 8. LCB and Complex Sphingolipid Content of *tsc10a-2*, *tsc10b-2*, and the Wild Type.

(A) LCBs and LCB phosphates (LCB-P) were extracted from etiolated hypocotyls of wild-type and mutant plants. LCBs analyzed included 3-KDS, DHS (d18:0), DHS:1Δ4 (d18:1), DHS:2Δ4,8 (d18:2), PHS (t18:0), PHS:1Δ8, (t18:1) and their phosphates. dw, dry weight.

(B) Analysis of the complex sphingolipids ceramide, hydroxyceramide, glucosylceramide, and glycosyl inositolphosphoceramide (GIPC). Data represent the mean of five biological replicates per genotype ± SE. Letters indicate statistically different groups using one-way ANOVA with groupings by Tukey's HSD using a 95% confidence interval.

reductase activity causes the leaf ionomic phenotype observed in *tsc10a*, we performed reciprocal root and shoot grafting experiments between the wild type and *tsc10a-1.* Self-grafted wild-type and *tsc10a* plants showed the same leaf ionomics profile as nongrafted plants (Figure 9A), establishing that grafting did not significantly affect the leaf concentrations of Na, Mg, K, Ca, Fe, Rb, and Mo, the elements known to be altered in *tsc10a*. Furthermore, grafted plants with a wild-type shoot and *tsc10a-1* mutant root had a leaf ionome indistinguishable from the *tsc10a-1* (Figure 9A) for Na, Mg, K, Ca, Fe, Rb, and Mo. This contrasts with grafted plants with a *tsc10a-1* shoot and wild-type roots, in which the leaf concentration of Na, Mg, K, Ca, Fe, Rb, and Mo was indistinguishable from the wild type (Figure 9A). Furthermore, when individual plants were grouped using unsupervised hierarchical clustering based on their total leaf ionome, all plants with *tsc10a-1* roots grouped together (Figure 9B), regardless of if they had a wild-type or *tsc10a-1* shoot. Such evidence clearly establishes that the leaf ionomic phenotype of *tsc10a-1* is driven by loss of 3-KDS reductase activity specifically in roots.

Roots of *tsc10a* Contain Increased Suberin in the Endodermis

We recently observed that elevated suberin in roots of the *enhanced suberin1* (*esb1*) *Arabidopsis* mutant is associated with significant alterations of the leaf ionome, including reductions in Ca and increases in Na and K (Baxter et al., 2009). To assess if a similar mechanism may be involved in the leaf ionomic phenotype of *tsc10a*, we quantified the aliphatic suberin monomers in roots of *tsc10a-1*, *tsc10a-2*, and the wild type (Figure 10), and the significance of any changes was determined using a single-factor mixed effect model ANOVA with a Benjamini-Hochberg multiple testing correction. We further imposed the requirement that a change in concentration of a suberin monomer be significant in multiple independent alleles. This analysis revealed significant ($P \leq 0.01$) increases in various suberin aliphatic monomers, including acids (20:0, 22:0, and 24:0), ω-OH acids (18:0, 18:1, 18:2, 20:0, and 22:0), dioic acids (18:0, 18:1, and 20:0), and alcohols (18:0, 20:0, and 22:0). These changes in individual aliphatic monomers represent an increase in the amount of total aliphatic monomers of 27% in both the

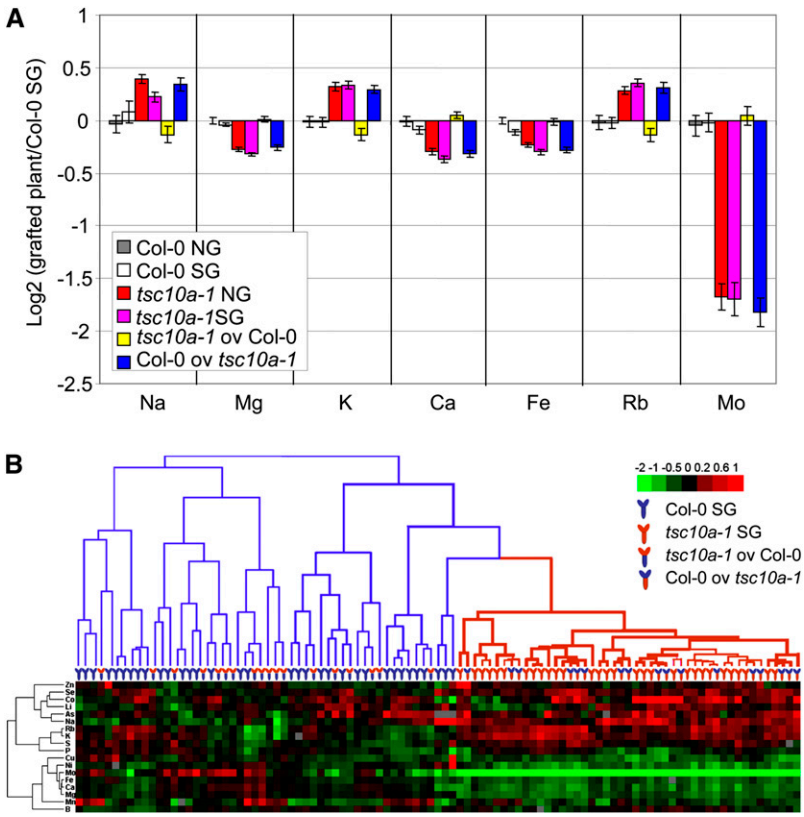

Figure 9. In *Arabidopsis*, the Root Determines the Ionomic Phenotype of the *tsc10a* Mutants.

(A) Comparison of the leaf ionome of grafted and nongrafted plants. Data treated as in Figure 3. Data represent means ± SE from $n = 18$ plants per graft type.

(B) Hierarchical clustering of grafting plants of Col-0 and *tsc10a-1*. Clustering was performed on the log2 ratio of each line versus the mean of nongrafted wild type. NG, nongrafted plants; SG, self-grafted plants; ov, over (e.g., Col-0 ov *tsc10a-1* represents plants with wild-type shoot grafted to a mutant root).

tsc10a-1 and *tsc10a-2* mutants. To further understand the effect that loss of 3-KDS reductase activity has on the amount and localization of suberin in *tsc10a-1*, we performed transmission electron microscopy (TEM) on roots of *tsc10a-1* and the wild type (Figure 11). Generally, in *Arabidopsis* roots, suberin is visible in the endodermis as alternating electron-opaque and electron-translucent layers inside the primary cell wall (Nawrath, 2002). In the TEM images presented here of *Arabidopsis* wild-type roots, suberin is clearly visible as alternating electron-opaque and electron-translucent layers on the inside of both the inner tangential cell wall and radial cell walls of the endodermis (Figure 11). However, wild-type plants lack suberin on the outer tangential cell wall of the endodermis (Figure 11). This contrasts with the endodermis of *tsc10a-1*, which clearly contains suberin on all sides of the cell wall (Figure 11).

Roots of *tsc10a* Respond Transcriptionally to Fe Deficiency

Leaves of *tsc10a* show reduced Fe accumulation of ~20% compared with the wild type (Table 1), and this reduced accumulation of Fe is reflected in a reduction in growth and increased chlorosis of *tsc10a* (*tsc10a-1* and *tsc10-2*) when grown in alkaline soils in which Fe has reduced bioavailability (Figures 12A and 12B). Furthermore, these growth defects in *tsc10a* are suppressed by the addition of extra Fe to the soil, confirming the Fe specificity of these phenotypes. To further understand the mechanism driving the reduced leaf Fe and impaired growth in alkaline soils observed in *tsc10a*, we measured the expression of *IRT1*, the Fe transporter known to be primarily responsible for Fe uptake in roots of *Arabidopsis* (Vert et al., 2002). Expression of *IRT1*, quantified using qRT-PCR, was observed to be elevated in roots of *tsc10a* compared with the wild type when grown under Fe-sufficient conditions (Figure 12C). Such evidence strongly supports the conclusion that roots of *tsc10a* are responding to Fe deficiency compared with wild-type roots. Interesting, although *IRT1* expression is elevated in roots of *tsc10a*, plasma membrane IRT1 protein accumulation remains at wild-type levels (Figure 12D).

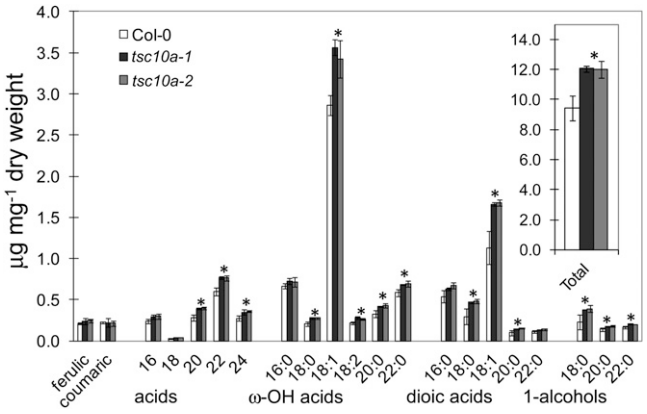

Figure 10. Mutation of *TSC10A* Leads to Increased Aliphatic Suberin Monomers in Roots of *Arabidopsis.*

Data represent means (n = 3 to 4) ± SD. Stars represents suberin monomers significantly different ($P \leq 0.01$) from the wild type for both *tsc10a-1* and *tsc10a-2* using a single-factor mixed effect model ANOVA with a Benjamini-Hochberg multiple testing correction.

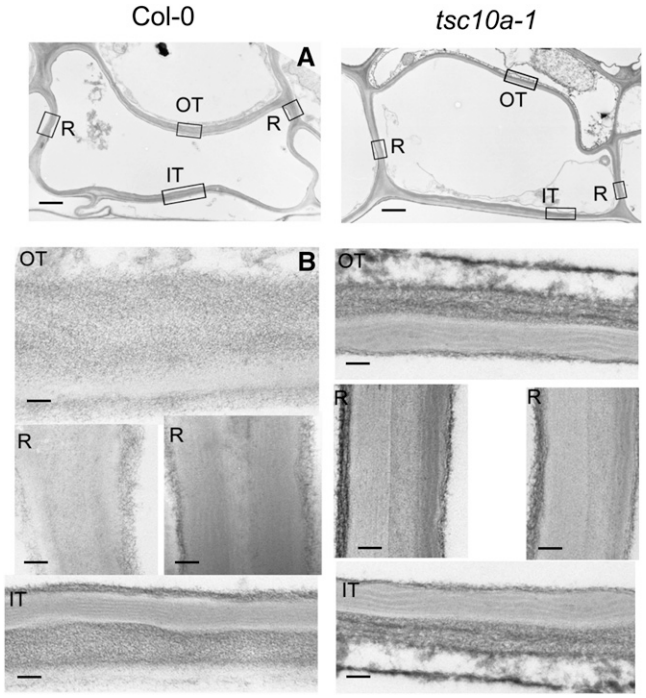

Figure 11. Loss of Function of *TSC10A* Leads to Altered Deposition of Suberin in Roots of *Arabidopsis.*

Suberin is visible as alternating electron-opaque and electron-translucent layers inside the primary cell wall. OT, outer tangential cell wall; IT, inner tangential cell wall; R, radial cell wall.
(**A**) Whole cells. Bar = 500 nm.
(B) Enlargement of areas indicated in **(A)**. Bar = 100 nm.

DISCUSSION

The results from this study conclusively establish that *TSC10A* (At3g06060) and *TSC10B* (At5g19200) from *Arabidopsis* encode 3-KDS reductases involved in the second step in sphingolipid biosynthesis. In addition, the observation that mutant plant lines lacking either *TSC10A* or *TSC10B* have no major growth defects under standard growth conditions, while plants lacking both genes are not recoverable, indicates that they are functionally redundant, and loss of both genes is lethal. The lethality of the *tsc10a tsc10b* double mutant confirms the essentiality of 3-KDS for sphingolipid biosynthesis. In previous studies, we have shown that plants with reduced sphingolipid biosynthesis are small due to impaired cell expansion (Chen et al., 2006; Dietrich et al., 2008). Therefore, it was surprising that plants lacking *TSC10A*, which is expressed at significantly higher levels than *TSC10B* (Figure 3), were visibly similar to the wild type. Since the specific activity of yeast-expressed *TSC10B* was considerably higher than that of yeast-expressed *TSC10A*, it was important to compare the 3-KDS reductase activity in the *tsc10a* mutant

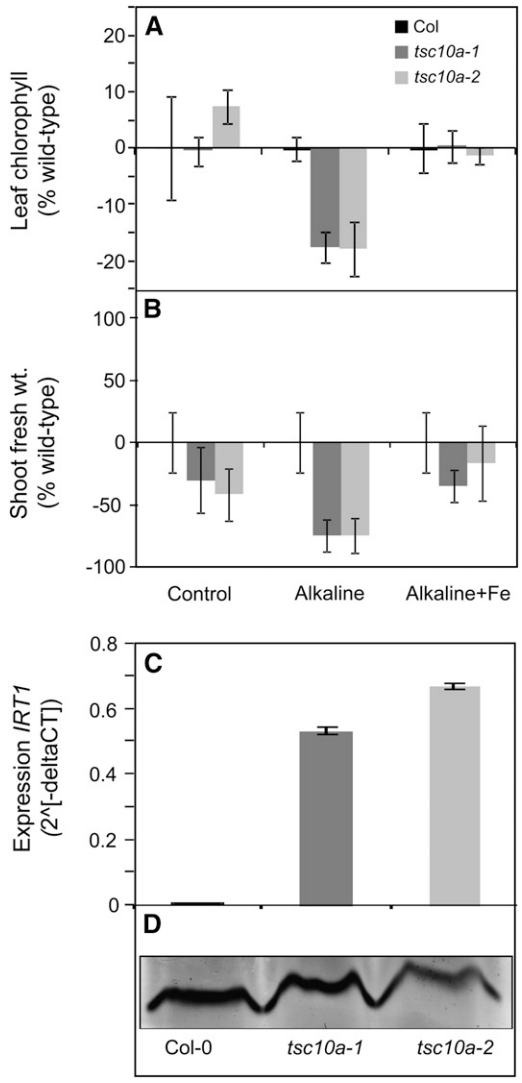

Figure 12. Iron Homoeostasis Is Disrupted in *Arabidopsis tsc10a* Mutants.

(A) and **(B)** Wild-type Col-0, *tsc10a-1*, and *tsc10a-2* plants grown on acidic soil, pH 5.6, alkaline soil, pH 7.9, or alkaline soil amended with Fe and plant vigor estimated by measuring leaf chlorophyll content **(A)** and plant fresh weight **(B)**. Values represent a mean (n = 3) ± SD.

(C) Quantification of the steady state levels of *IRT1* mRNA by qRT-PCR in roots of *tsc10a*. *Ubc* was used as the control gene, and four PCR reactions were done per replicate using three independent biological samples per genotype with error bars representing SD.

(D) Analysis by immunoblotting of IRT1 protein in the plasma membrane of roots of wild-type, *tsc10a-1*, and *tsc10a-2* plants. Each lane was loaded with equal quantities of PM measured as 1.5 μg of total protein.

plants to that in the *tsc10b-1* mutant plants. The results showed that *tsc10a-2* plants have far less (<5%) 3-KDS reductase activity than either *tsc10b-2* or wild-type plants (Figure 7), establishing that *TSC10A* encodes the majority (>95%) of the 3-KDS reductase activity in *Arabidopsis*. It is interesting to note that expression of *TSC10A*, and activity of 3-KDS reductase, is enhanced in the *tsc10b* mutants (Figures 2 and 7), suggesting that loss of *TSC10B* is compensated for by elevated *TSC10A* expression. This compensatory increase in *TSC10A* expression and 3-KDS reductase activity may be the explanation for the reversed leaf ionomic phenotype for K, Ca, Rb, and Mo observed in *tsc10b* mutant, compared with *tsc10a* (Tables 1 and 2).

In contrast with other characterized 3-KDS reductases, which stereoselectively reduce 3-KDS to form D-erythro-DHS, TSC10A was found to produce both D-erythro- and L-threo-DHS (Figure 5). It is interesting to note that both of the *Arabidopsis* enzymes are able to use either NADPH or NADH as cofactor, but it is only with NADPH that TSC10A produces both the L-threo and D-erythro products. Based on the structures of many SDRs, it is known that the N-terminal part of the protein contains the Rossmann fold that binds the NAD(P)H cofactor, whereas the C-terminal region forms the substrate binding domain. In addition, features of the Gly motif within the Rossmann fold predict which cofactor a given SDR is likely to use (Kallberg and Persson, 2006). The *Arabidopsis* enzymes are most closely aligned with those SDRs that use NADPH, but a conserved Arg is missing. In future studies, it will be interesting to construct chimeric proteins in which the relevant domains of TSC10A and TSC10B are swapped to gain insight into what controls the stereoselectivity of the enzymes. It is worth pointing out that the nonphysiological L-threo-DHS, also called safingol, has been shown to have anticancer activity (Morales et al., 2007). It would therefore be of potential value to create a 3-KDS reductase with reversed stereoselectivity.

Despite the ability of the *Arabidopsis* 3-KDS reductases to substitute for Tsc10p in yeast, the enzymes have different topologies. Several hydropathy algorithms were used to determine the location of potential TMDs in the proteins (see Supplemental Table 1 online). All of the programs predict that residues 285 to 305 of Tsc10p comprise a TMD, and based on the results presented that place both ends of the protein in the cytoplasm, we conclude that there must be an even number and, thus, probably one additional TMD. The presence of additional TMDs located between amino acids 160 to 180 and 255 to 275 is predicted by several programs, but the hydrophobic domain from 160 to 180 includes two of the conserved catalytic residues (Ser-167 and Tyr-180) and is therefore unlikely to lie within the membrane. We therefore favor a topology model for Tsc10p with a TMD between 255 to 275, a short luminal loop, and a second TMD at 285 to 305 as we have previously proposed (Gupta et al., 2009). We also showed previously that the C-terminal 38 amino acids of Tsc10p are not required for enzymatic activity (Beeler et al., 1998). The *Arabidopsis* 3-ketosphinganine reductases have two predicted TMDs near their C termini that are positioned analogously to those in Tsc10p, but they also have a highly hydrophobic N-terminal extension for which there is no counterpart in Tsc10p. Furthermore, in contrast with Tsc10p, the glycosylation data for TSC10A clearly indicate that there is an odd number of TMDs with the N terminus in the lumen and the C terminus in the cytoplasm. Our data also show that the N terminus of TSC10B is in the lumen, and although we did not experimentally confirm that the C terminus is cytoplasmic, given the high similarity between the two *Arabidopsis* enzymes, we presume that they both have an N-terminal TMD, a large

cytoplasmic catalytic domain followed by two additional closely spaced TMDs and a short cytoplasmic tail, a similar structure to that we previously proposed for the human 3-KDS reductase (FVT1) (Gupta et al., 2009). It is possible that the heterologously expressed *Arabidopsis* proteins adopt a non-native topology in yeast. However, these studies likely provide an accurate picture of the in planta topology because the plant enzymes are more similar to the human 3-KDS reductase (FVT1) than to Tsc10p, and topology studies of FVT1 in mammalian cells agree with the results presented for the *Arabidopsis* enzymes (Gupta et al., 2009). Furthermore, the heterologously expressed *Arabidopsis* 3-KDS reductases both have higher specific activities than yeast Tsc10p, also arguing that they adopt their native membrane topologies.

Although *Arabidopsis* plants lacking the *TSC10A* gene that encodes the majority of 3-KDS reductase activity only show subtle growth defects (see Supplemental Figures 1 to 3 online), the leaf ionome of *tsc10a* mutant plants is significantly perturbed, with increases in the concentrations of Na, K, and Rb and decreases in Mg, Ca, Fe, and Mo (Table 1). The leaf ionomic phenotype of *tsc10a-1* was initially used to identify the *TSC10A* gene by map-based cloning of the *7113* ionomic mutant (here referred to as *tsc10a-1*), identified in a previous screen of fast neutron mutagenized *Arabidopsis* (Lahner et al., 2003). Analysis of three independent loss-of-function alleles of *TSC10A* (*tsc10a-1*, *tsc10a-2*, and *tsc10a-3*) and complementation with the wild-type *TSC10A* allele confirmed that loss of function of *TSC10A* causes the observed leaf ionomic phenotype (see Supplemental Figures 4 and 5 online; Figure 1). Reciprocal grafting of roots and shoots from *tsc10a-1* and wild-type plants established that, even though *TSC10A* is expressed throughout the plant, the leaf ionomic phenotype of the *TSC10A* loss-of-function mutants is driven by loss of 3-KDS reductase activity solely in the roots (Figures 3 and 9). Grafted plants lacking 3-KDS reductase activity in shoots (*tsc10a-1* shoot/wild-type root) had wild-type leaf ionomes, whereas grafted plants lacking 3-KDS reductase activity in roots (wild-type shoot/*tsc10a-1* root) had a leaf ionome indistinguishable from the *tsc10a-1* mutant.

Ion transport from the soil, through the root, and into the shoot involves both movement through the apoplastic space between cells and movement through cells that requires transport across the plasma membrane (PM). The asymmetric deposition of suberin in the endodermis blocks the apoplastic pathway, limiting access to the xylem and phloem to only those ions moving symplastically. Furthermore, the asymmetric arrangement of influx and efflux ion transporters on the PM in cells of the epidermis, endodermis, and stele drives the unidirectional transport of ions through the symplastic pathway. Depending on which ion is being transported the apoplastic or symplastic transport pathways in the root can predominate. Recently, we established that a substantial proportion of Ca transported to the shoot in *Arabidopsis* moves through the root apoplast, since a doubling of suberin in the root apoplast was observed to cause an ~50% reduction in leaf Ca accumulation (Baxter et al., 2009). By contrast, only a minor change in leaf Fe was observed (~9%) (Baxter et al., 2009), suggesting that apoplastic transport of Fe is limited. This lack of an apoplastic transport pathway for Fe is confirmed by the fact that the PM localized Fe transporter IRT1 is the only pathway for Fe uptake from soil in *Arabidopsis*; loss of IRT1 in *Arabidopsis* is lethal (Vert et al., 2002).

Similar to the elevated suberin in *esb1*, we also observed elevated suberin in roots of the *tsc10a* mutant (Figure 10). Furthermore, the suberin in *tsc10a* was observed to be distributed uniformly around cells of the endodermis, unlike wild-type roots where suberin is generally found only on the inner tangential cell wall and radial cell wall of endodermal cells (Figure 11). We conclude that it is the elevated suberin, along with its enhanced distribution, in the wall of endodermal cells that is responsible for blocking apoplastic transport of Ca^{2+} in *tsc10a* roots, giving rise to the ~20% reduction of leaf Ca observed in the mutant. The 20% reduction in leaf Ca observed in *tsc10a* is less than the 50% reduction observed in *esb1* (Baxter et al., 2009), and this likely reflects the fact that suberin in *tsc10a* is increased by 27% compared with the 100% increase observed in *esb1* (Baxter et al., 2009). The elevated suberin in *tsc10a* may also be responsible for the enhanced Na, K, and Rb observed in the mutant, since similar changes were also observed in the *esb1* mutant (Baxter et al., 2009). One possible mechanism to explain the elevated leaf Na and K may be that increased resistance to Na^+ and K^+ transport via the apoplastic pathway increases the movement of these ions via a more efficient symplastic transport pathway mediated by high affinity transporters, such as the Na transporter HKT1 (Uozumi et al., 2000) and the K transporters HAK5 and AKT1 (Rubio et al., 2008). We are currently unsure if reduced Mg in *tsc10a* is related to the changes in suberin observed in this mutant, since leaf Mg is unchanged in *esb1* (Baxter et al., 2009). However, there is substantial evidence showing that in plants, leaf Mg and Ca are broadly correlated across taxa (Broadley et al., 2004; Watanabe et al., 2007) and also specifically in *Arabidopsis* (Broadley et al., 2010; Buescher et al., 2010). The mechanism underlying this coregulation of Mg and Ca in plants is yet to be established. A better understanding of the contrasting leaf Mg and Ca accumulation between *esb1* and *tsc10a* could provide a powerful tool to help resolve this important unanswered question. Interestingly, similar to *esb1* (Baxter et al., 2009) the *TSC10A* loss-of-function mutants also show increased resistance to wilting (see Supplemental Figure 7 online).

Recent discoveries, such as the determination that acyl-CoA: glycerol-3-phosphate acetyltransferase, cytochrome P450 fatty acid ω-hydroxylase CYP86A1, β-ketoacyl-CoA synthase, fatty acyl-CoA reductases (FAR1, FAR4, and FAR5), a distinct glycerol-3-phosphate acyltransferase, and the DSO/ABCG11 transporter are involved in suberin deposition are starting to unravel the enzymology of suberin biosynthesis (Beisson et al., 2007; Li et al., 2007; Höfer et al., 2008; Franke et al., 2009; Domergue et al., 2010; Panikashvili et al., 2010; Yang et al., 2010). The recent observation that loss of function of the dirigent-like protein *ESB1* in *Arabidopsis* causes a doubling of suberin (Baxter et al., 2009) may provide the first evidence that dirigent-like proteins (Davin and Lewis, 2000) are involved in the biosynthesis of suberin, though currently the mechanism remains elusive. Though progress is being made understanding the biosynthesis of suberin, very little is known about the processes involved in transport of suberin monomers to the cell wall or the control of polymerization that leads to the highly regular lamellar structure visible

in TEM (Figure 11). Sphingolipids have been established to be enriched in microdomains, or lipid rafts, within the PM, and these lipid rafts have been shown to be enriched in specific proteins (Borner et al., 2005), including proteins thought to be involved in cell wall assembly, including SKU5 and SKS-1 (Sedbrook et al., 2002) and GPDL1 (Hayashi et al., 2008). It is possible that perturbations in PM lipid rafts in *tsc10a*, caused by the disruption of sphingolipid biosynthesis in this mutant, may alter the activity of such cell wall assembly proteins, and this may be responsible for the enhanced suberin biosynthesis observed in this mutant. However, further investigations are required to determine this.

Given that Fe is known to be primarily transported in the root symplast (Vert et al., 2002; Baxter et al., 2009), elevated suberin in *tsc10a* cannot explain the reduced leaf Fe and increased susceptibility to Fe deficiency in alkaline soils observed in *tsc10a-1* and *tsc10a-2* (Figures 12A and 12B). However, our grafting results establish that whatever mechanism is driving reduced leaf Fe in the *TSC10A* loss-of-function mutants it is based in the root (Figure 9). Expression of the Fe transporter *IRT1* is a good marker of Fe deficiency, since this gene is known to be strongly upregulated under Fe deficiency in roots of *Arabidopsis* (Connolly et al., 2002). *IRT1* expression in roots of *TSC10A* loss-of-function mutants is highly elevated compared with the Col-0 wild type (Figure 12C) when both plants are grown in soil containing sufficient Fe, establishing that *TSC10A* loss-of-function mutants are responding to Fe deficiency. The Fe concentration of leaves of the *TSC10A* loss-of-function mutants is reduced by ~20% compared with Col-0 wild type, and this reduction in leaf Fe is similar to the 26% reduction observed for the *frd3-5 Arabidopsis* mutant (Lahner et al., 2003). *frd3* is unable to load Fe-citrate into the xylem for translocation to the shoots (Durrett et al., 2007), leading to enhanced transcription of *IRT1*, increased accumulation of the IRT1 protein, and enhanced ferric chelate reductase activity in roots (reviewed in Morrissey and Guerinot, 2009). Based on the response of *frd3* to reduced leaf Fe, we conclude that roots of the *TSC10A* loss-of-function mutants are also responding to reduced leaf Fe by increasing expression of *IRT1*. Our conclusion that loss of 3-KDS reductase activity in the *TSC10A* loss-of-function mutants is causing Fe deficiency is also supported by the observation that Mo accumulation in leaves of the *TSC10A* loss-of-function mutants is reduced by 67% compared with the wild type, as this is consistent with the reduction in leaf Mo we observed in wild-type plants responding to Fe deficiency (Baxter et al., 2008b). Furthermore, we have previously shown that *frd3*, a mutant that displays constitutive Fe deficiency responses, also shows a similar reduction in leaf Mo concentration compared with the wild type (Lahner et al., 2003).

However, the mechanism whereby loss of 3-KDS reductase activity in the *TSC10A* loss-of-function mutants causes reduced leaf Fe accumulation is unclear. One possibility is that alteration in the composition of lipid rafts in roots of the *TSC10A* loss-of-function mutants is causing reduced IRT1 transport activity. Several types of ion transporters, including ABC transporters, aquaporins, a Ca-ATPase, and a cyclic nucleotide gated channel, have been identified in lipid rafts (Borner et al., 2005; Morel et al., 2006); however, we currently have no evidence that IRT1 is located within a lipid raft domain. Another possibility is that altered lipid raft structures in the *TSC10A* loss-of-function mutants may disrupt the asymmetric cellular localization of the various Fe transporters, including IRT1, FPN1, FPN2, and FRD3 (reviewed in Morrissey and Guerinot, 2009), required for the correct unidirectional transport of Fe from the root surface to the stele for translocation to the shoot.

Significantly, unlike in *frd3*, which accumulates high levels of IRT1 protein (Rogers and Guerinot, 2002), leading to increased shoot accumulation of Mn, Co, Zn, and Cd (Delhaize, 1996; Rogers and Guerinot, 2002; Lahner et al., 2003), we observe no such enhanced accumulation of IRT1 protein in roots (Figure 12D) or increased shoot accumulation of Mn, Co, Zn, and Cd in the *TSC10A* loss-of-function mutants. This is puzzling since roots of the *TSC10A* loss-of-function mutants show a clear increase in the steady state levels of *IRT1* mRNA. IRT1 is known to be subject to posttranslational regulation, with protein from the *IRT1* transcript only accumulating in roots of plants responding to Fe deficiency, even when expression is driven from the 35S promoter (Connolly et al., 2002; Kerkeb et al., 2008). Therefore, we propose that loss of 3-KDS reductase activity in the *TSC10A* loss-of-function mutants is disrupting the ability of the Fe deficiency signal, likely generated in the leaves, to suppress the Fe-induced turnover of IRT1 in roots. The signaling mechanism involved in the Fe-induced turnover of IRT1 is currently unknown. However, our results suggest that sphingolipids are involved in this signaling mechanism, either directly via a sphingolipid-related signaling molecule or indirectly by the disruption of critical protein interactions facilitated by lipid raft formation.

In summary, we show that *Arabidopsis* contains two bona fide 3-KDS reductases (TSC10A and TSC10B) that have redundant functions in sphingolipid biosynthesis. Both 3-KDS reductases are expressed throughout the plant, but TSC10A contributes >95% of the 3-KDS reductase activity in planta. Loss of both TSC10A and TSC10B is lethal. Both TSC10A and TSC10B are located in the ER and have both altered substrate stereospecificity and membrane topology compared with the yeast enzyme. However, both plant 3-KDS reductase can function in yeast. Furthermore, the loss of 3-KDS reductase activity in the *TSC10A* loss-of-function mutants leads to increases in the leaf concentration of Na, K, and Rb and decreases in Mg, Ca, Fe, and Mo. Changes in Ca, Na, and K are most likely due to the increased root suberin observed in the *TSC10A* loss-of-function mutants. However, the reduction in leaf Fe is more likely due to alterations in Fe transport caused by perturbations in PM sphingolipid-rich lipid raft structures. Although, significantly, the *TSC10A* loss-of-function mutants also appears impaired in the ability to inhibit Fe-induced turnover of IRT1, leading to a plant that is responding transcriptionally to Fe deficiency but that is unable to accumulate elevated levels of IRT1 protein.

METHODS

Plant Material and Growth Conditions

For axenic growth, *Arabidopsis thaliana* seeds were surface sterilized and sowed on Murashige and Skoog agar plates (Sigma-Aldrich) containing 1% sucrose. After 3 d of stratification at 4°C, the plates were maintained

at 16 h light/8 h dark at 120 μmol m^{-2} s^{-1} at 23°C. Soil-grown plants, except those for inductively coupled plasma (ICP) analysis, were maintained at 22°C and 50% humidity under either long-day conditions with a 16-h-light (100 μmol m^{-2} s^{-1})/8-h-dark cycle or short-day conditions with an 8-h-light (200 μmol m^{-2} s^{-1})/16-h-dark cycle.

Arabidopsis plants for ICP–mass spectrometry analysis were grown in a controlled environment that has been described before (Lahner et al., 2003). Briefly, seeds were germinated on a 20-row tray with moist soil (Pro-Mix; Premier Horticulture) after stratification at 4°C for 3 d. The plants were then grown with 10 h light (90 μmol m^{-2} s^{-1})/14 h dark and 19 to 22°C temperature. During the following days, plants were bottom-watered twice a week with modified 0.25× Hoagland solution (Baxter et al., 2009). Several leaves were harvested from 5-week-old plants for elemental analysis.

Plant transformation was achieved using the floral dipping method (Clough and Bent, 1998). Transgenic lines were selected on either half-strength Murashige and Skoog media or soil with hygromycin or BASTA according to the selection marker used in the transformation. For the hypocotyl elongation experiment, seeds were grown on square Petri plates (100 × 15 mm). After stratification, plates were placed in the light for 6 to 8 h to promote germination. Plates were then wrapped in foil and stored vertically at 22°C for 5 d prior to measurement of hypocotyls lengths.

Yeast Growth

Standard yeast media were prepared and yeast was cultured according to established procedures (Sherman et al., 1986). The *tsc10Δ* and *tsc10-1* mutant yeast strains, *Mat**a** tsc10Δ::TRP1 ura-352 trp1Δ ade2 his4 leu2Δ* and *Matα tsc10-1 leu2Δ trp1Δ ura3*-52, were described previously (Beeler et al., 1998). The *tsc10Δ* mutant cells were cultured in medium containing 15 μM PHS and 0.2% tergitol. The plasmids expressing the *Arabidopsis* Tsc10p orthologs were tested for their ability to complement the yeast *tsc10* mutants by streaking transformants onto YPD with and without PHS.

Tissue Elemental Analysis

Tissue samples were dried at 92°C for 20 h in Pyrex tubes (16 × 100 mm) to yield ~2 to 4 mg of tissue for elemental analysis. After cooling, seven of 108 samples from each sample set were weighed. All samples were digested with 0.7 mL of concentrated nitric acid (OmniTrace; VWR Scientific Products) and diluted to 6.0 mL with 18 MΩ water. Elemental analysis was performed with an ICP–mass spectrometer (Elan DRCe; Perkin-Elmer) for Li, B, Na, Mg, P, S,K, Ca, Mn, Fe, Co, Ni, Cu, Zn, As, Se, Mo, Rb, and Cd. All samples were normalized to calculated weights, as determined with a heuristic algorithm using the best-measured elements, the weights of the seven weighed samples, and the solution concentrations described by Lahner et al. (2003) and implemented in the PiiMS database (Baxter et al., 2007). An Excel implementation of this algorithm is available at www.ionomicshub.org along with validation data sets. The normalized data were deposited in the PiiMS database (Baxter et al., 2007), which can be downloaded from www.ionomicshub.org.

Map-Based Cloning of *tsc10a-1*

DNA microarray-based bulk segregant analysis was performed as previously described (Borevitz et al., 2003; Hazen et al., 2005). Briefly, SFPs were identified between Col-0 and L*er*-0 by hybridizing labeled genomic DNA from each of the accessions to Affymetrix ATTILE 1.0R microarrays. Two genomic DNA pools from an F2 population of a cross between L*er*-0 and the *tsc10a-1* mutant in the Col-0 background were created and hybridized to separate DNA microarrays. Each one of the pools contained plants with either shoot Ca and Mg contents similar to Col-0 (control pool) or low shoot Ca and Mg contents similar to *tsc10a-1* (low Ca and Mg pool). At loci unlinked to the low Ca and Mg phenotype, the pools should have equivalent amounts of each genotype, and the hybridization signal at each SFP should be intermediate between the two parent accessions, for an average difference between the two DNA microarrays of zero. At linked loci, the difference between the two DNA pools should be approximately two-thirds the difference between the parent accessions. By smoothing the signal across multiple SFPs, noise is reduced and the peak of the differences in hybridization signal will correspond to the chromosomal region of the loci controlling the low Ca and Mg trait. Raw hybridization data (.CEL files) for each probe on the ATTILE 1.0R DNA microarrays used in these experiments have been submitted to the Gene Expression Omnibus and are accessible through GEO Series accession numbers (http://www.ncbi.nlm.nih.gov/geo/query/acc.cgi?acc=GSE15655). PCR-based genotyping was used for further mapping of the causing mutation in *tsc10a-1*. Using four SSLP markers and a population of 241 F2 plants from the L*er*-0 × *tsc10a-1* cross, we were able to map the gene to within a 400-kb genomic region. Further SSLP and cleaved-amplified polymorphic sequence markers were developed within this 400-kb mapping interval and used to screen 1279 further L*er*-0 × *tsc10a-1* F2 plants to identify informative recombinants to further narrow the mapping interval to a 30-kb region between cleaved-amplified polymorphic sequence markers of T1818K and T1848K. Overlapping fragments of ~0.7 to ~1 kb each, covering this 30-kb candidate region, were amplified from genome of *tsc10a-1* and sequenced. The sequence of these fragments was alignment with the wild-type sequence using DNASTAR. All primers for molecular markers and sequences are listed in Supplemental Table 2 online.

Arabidopsis Grafting

Seedlings were grafted and grafted seedlings grown in soil as previously described (Rus et al., 2006). Plants were harvested for leaf elemental analysis 4 weeks after transfer to soil.

Plasmid and Transgene Preparation

For construction of yeast expression vectors, *TSC10A* and *TSC10B* were PCR amplified from an *Arabidopsis* cDNA library (Paul et al., 2006) using primers At3g06060 sense and At3g06060 antisense, and At5g19200 sense and At5g19200 antisense (see Supplemental Table 2 online). The amplified fragments were restricted with either *Xho*I or *Sal*I and ligated into the *Sal*I site of plasmid pADH-3X-HA (Kohlwein et al., 2001), resulting in an in-frame fusion of the N-terminal triple-HA tag to the TSC10 candidate genes cloned behind the constitutive ADH1 promoter for yeast expression. For topology studies, the 53–amino acid GC from Suc2p was inserted after the start codon (GC@2) or before the stop codon in the TSC10A or TSC10B expression plasmid using the same strategy used for the topology studies of Lcb1p (Han et al., 2004).

For complementing the *tsc10a* mutants, an ~5-kb wild-type genomic DNA fragment including the promoter and open reading frame of *TSC10A* was PCR amplified using primers of AtTSC10ACS and AtTSC10ACA (see Supplemental Table 2 online), and the PCR fragment was restricted with *Asc*I and cloned into the binary vector pEC291 (Curtis and Grossniklaus, 2003) to produce EC291-TSC10Ag. The final plasmid was transformed into *Agrobacterium tumefaciens* strain of GV3101 and was introduced into *Arabidopsis* using the floral dip method (Clough and Bent, 1998).

For construction of the vectors for transient expression of the GFP-TSC10A or GFP-TSC10B fusion proteins, a DNA fragment containing the complete coding region of *TSC10A* or *TSC10B* was amplified from *TSC10A* cDNA using TSC10A_GFP_S and AtTSC10A_GFP_A primer pairs or TSC10BGFTF and TSC10BGFTR primer pairs (see Supplemental

Table 2 online). The amplified PCR product for *TSC10A* was ligated into the binary vector p1301A7 using the *Xba*I and *Bam*HI restriction sites in frame with the GFP coding sequence. The p1301A7 plasmid was modified from pCAMBIA1301 by the insertion of a DNA fragment containing the GFP coding sequence, with the stop codon removed, two multicloning sites added at the 5′ and 3′ ends, and a NOS terminated added at the 3′ end. The PCR product for *TSC10B* was cloned into pMDC43 (Curtis and Grossniklaus, 2003) in frame with the GFP coding sequence using the Gateway recombinational cloning strategy.

Subcellular Localization of TSC10A and TSC10B

The subcellular localization of TSC10A and TSC10B was achieved by the transient expression of GFP-tagged proteins in tobacco (*Nicotiana tabacum*) BY-2 protoplasts. Tobacco BY-2 culture cells were digested in protoplast isolation solution (1.2% Cellulase R10 and 0.6% Macerozyme, pH 5.7) for 4 h at room temperature. Digested cells in the isolation solution were layered on top of a solution containing 0.01% myo-inositol, 0.29% L-proline, 0.01% enzymatic casein hydrolysate, 10% sucrose, 0.098% MES, 0.43% Murashige and Skoog salts, 0.001% vitamin B1, and 0.037% KH_2PO_4, pH 5.7, and protoplasts collected from the top of the solution after low-speed centrifugation. The *GFP-TSC10A* or *GFP-TSC10B* and ER maker *CD3-959-mCherry* constructs were cotransformed into tobacco protoplasts using the polyethylene glycol transformation method (Hwang and Sheen, 2001). Fluorescence from GFP and mCherry was observed using a confocal microscope (Zeiss LSM 710) 36 to 48 h after transfection.

Yeast Membrane Preparation

Microsomes were prepared from exponentially growing cells as previously described (Paul et al., 2006). Briefly, cells were pelleted at 5000*g*, washed with water, and repelleted. Cell pellets were resuspended in TEGM (0.05 M Tris, pH 7.5, 1 mM EGTA, 1 mM β-mercaptoethanol, 1 mM phenylmethylsulfonyl fluoride, 1 μg/mL leupeptin, 1 μg/mL pepstatin A, and 1 μg/mL aprotinin) buffer at 1 mL/50 OD cells, and glass beads (0.5-mm diameter) were added to the meniscus. Cells were disrupted by four cycles of vortexing for 1 min followed by cooling on ice for 1 min, and pelleted at 8000*g* for 10 min. The supernatant was transferred to a fresh tube and centrifuged at 50,000*g* for 30 min. The resulting pellet was resuspended by Dounce homogenization in at least a 10× volume of TEGM buffer and repelleted at 50,000*g*. The final membrane pellet was resuspended in TEGM buffer containing 33% glycerol and stored at −80°C.

Plasma Membrane Purification

Plasma membrane was purified from *Arabidopsis* root tissue according to Gustin et al. (2009). First, 8 to 10 g fresh weight of root was collected from 6-week-old plants grow in soil and thoroughly washed in deionized water. Roots were homogenized in grinding buffer (25 mM HEPES-KOH, pH 8.5, 0.29 M sucrose, 3 mM DTT, 2 mM EDTA, 0.5% polyvinylpolypyrrolidone, 0.1 mM phenylmethylsulfonyl fluoride, and protease inhibitor cocktail) using a mortar and pestle with acid-washed sand at 4°C. After homogenization, the homogenate was filtered through miracloth and reextracted three further times. The combined supernatant was centrifuged at 10,000*g* for 10 min, and the supernatant transferred to a new tube and centrifuged at 100,000*g* for 1 h to collect the microsomal membrane fraction. The microsomal membrane pellet was resuspended in suspension buffer (0.33 M sucrose, 3 mM KCl, and 5 mM potassium phosphate, pH 7.8). The suspended microsomal membranes was added to a mixed two phase system containing 6.6% (w/w) Dextran T-500, 6.6% (w/w) polyethylene glycol 3350, 0.33 M sucrose, 3 mM KCl, and 5 mM potassium phosphate, pH 7.8. The phase system was thoroughly mixed by gentle inversion 100 times. The mixed phase was then separated by centrifugation at 1500*g* for 5 min. The upper phase, which contains most of the PM, was subsequently reextracted for three further times with fresh lower phase from a bulk phase system of identical composition prepared separately. The final upper phase was diluted 10 times in suspension buffer, and the PMs were collected by centrifuge at 100,000*g* for 1 h. Protein concentrations were estimated using the BCA protein assay kit (Pierce) and the PM analyzed by immunoblotting.

Immunoblotting

Microsomal proteins (15 μg) from strains expressing the HA-Tsc10p and the candidate HA-tagged TSC10 proteins were resolved on a 4 to 12% BIS-TRIS PAGE (Invitrogen). Following transfer of the separated proteins to nitrocellulose, the blots were blocked in 0.1 M Tris, 0.15 M NaCl, 0.1% Tween 20, and 5% dry milk. HA-tagged proteins were detected using horseradish peroxidase–conjugated monoclonal anti-HA antibodies (Roche Molecular Biochemicals) at 1/1000. The bound antibodies were detected by the enhanced chemiluminescence protein gel blotting detection system (Amersham Biosciences). For analysis of plasma membrane proteins, aqueous two-phase purified PM were mixed with 6× SDS loading buffer with 100 mM DTT and incubated at room temperature for 10 min. Samples were resolved by SDS-PAGE and electroblotted to a polyvinylidene fluoride membrane and membranes incubated with primary antibodies and horseradish peroxidase–conjugated secondary antibodies using standard protocols.

Long-Chain Base Analysis of Yeast

Yeast *tsc10-1* mutant cells harboring the pADH-HA expression plasmids were grown in SD medium (0.67% yeast nitrogen base and 2% glucose) lacking Leu to an A_{600} of ~1.0. Fifty A_{600} units of cells were beaten with glass beads in 1.2 mL 0.5 M NH_4OH for 4 min. Six milliliters of $CHCl_3$:methanol (1:2) were added, and following centrifugation to remove cellular debris and beads, the cleared supernatant was transferred to a fresh tube. Three milliliters of $CHCl_3$ were added, the sample was vortexed, and small volumes of $CHCl_3$:methanol (1:2) were added until the solution cleared. Six milliliters of 0.5 M NH_4OH was added, and the sample was vortexed and centrifuged and the upper layer was removed. The lower layer was washed several times with 60 mM KCl until completely clear. The cleared layer was dried under N_2 and resuspended in 100 μL $CHCl_3$. Thirty microliters of the extracted lipids were applied to the preadsorbent area of a Silica 60 TLC plate (AnalTech) and developed in $CHCl_3$:methanol: 2 M NH_4OH (40:10:1). After drying, the plate was sprayed with 0.2% ninhydrin in 95% ethanol and mildly heated until developed. Authentic standards (90 pmol 3-KDS, Matreya; 60 pmol PHS or DHS, Sigma-Aldrich) were added directly to the plate before development.

3-KDS Reductase Assay

3-KDS reductase was assayed as previously described (Beeler et al., 1998) using [^{14}C]-3KDS and [^{3}H]-3-KDS prepared with soluble 6-His-tagged *Sphingomonas paucimobilis* SPT expressed in *Escherichia coli* and purified by Ni-NTA chromatography, palmitoyl-CoA, and [^{14}C]- or [^{3}H]-Ser (Gupta et al., 2009). Extracted LCBs were dried, suspended in $CHCl_3$:methanol (2:1, v/v), and resolved on a Silica Gel G TLC plate developed with $CHCl_3$:methanol:2 M NH_4OH (40:10:1). [^{3}H]-3-KDS and [^{3}H]-DHS (identified by ninhydrin-stained unlabeled standards resolved in an adjacent lane) were scraped, and radioactivity determined by liquid scintillation spectrometry. [^{14}C]-3KDS and [^{14}C]-DHS were quantified using a STORM 860 phosphor imager (Amersham). For determination of

the specific activities of the enzymes, the amount of 3X-HA-tagged Tsc10p, TSC10A, and TSC10B was determined by comparison to purified 3X-HA tagged *S. paucimobilis* SPT using scanning densitometry of immunoblots.

Analysis of AccQ-Derivatized LCBs

LCBs and complex sphingolipids from the in vitro 3-KDS reductase assays or standards were dried under N_2 and dissolved in methanol:190 mM triethylamine (20:3). AccQ derivitization solution (AccQ-Fluor; Waters) was added at 2 mM and allowed to react at room temperature for 60 min. Methanolic KOH (0.1 M) was added and allowed to react at 37°C for 30 min, and the solution was then neutralized by the addition of methanolic acetic acid (final 0.1 M). A portion of this reaction mixture was injected onto a reverse phase C18 column (Jones Chromatography) using an HP1090 HPLC with an autosampler at 1.5 mL/min acetonitrile: methanol:water:acetic acid: triethylamine (48:32:13.5:3:0.7), solution A. After 60 min, the column was flushed and reset using acetonitrile: methanol (60:40) at 1.0 mL/min for 10 min and returned to solution A at 1.5 mL/min for 6 min. The AccQ-derivatized products were detected by an HP fluorescence detector set at 244 nm as the excitation wavelength and 398 nm as the emission wavelength.

Arabidopsis Microsomal Membrane Preparation and 3-KDS Reductase Assays

Plant microsomes from wild-type *Arabidopsis* and *tsc10a* and *tsc10b* mutants were prepared as described previously (Chen et al., 2006). ^{3}H-3-KDS was added (40,000 cpm, ~20 μM) to a 300- μL reaction mixture containing 0.05 M HEPES, pH 6.9, 2 mM NAD(P)H, 0.25% tergitol, and 2 mM β-mercaptoethanol. The reaction was initiated by the addition of 0.5 mg microsomal protein prepared from the wild type and *tsc10a-2* and *tsc10b-1* mutants. After 30 min at 37°C, the reaction was stopped by addition of 100 μL 2 N NH_4OH and 2 mL of CH_3Cl:methanol (1:2). The LCBs were extracted and resolved by thin layer chromatography as described above. Controls included reactions lacking microsomal protein, reactions lacking NAD(P)H cofactor, reactions with microsomal protein prepared from the *tsc10Δ* cells, and chemical reduction using 60 mM $NaBH_4$.

Sphingolipid Profiling of Wild-Type and Mutant *Arabidopsis*

The sphingolipid profiles of elongating hypocotyls from wild-type, *tsc10a-2*, and *tsc10b-2* mutant plants was performed by reversed-phase high performance liquid chromatography coupled to electrospray ionization–tandem mass spectrometry detection as previously described (Markham et al., 2006; Markham and Jaworski, 2007). The 3-KDS was detected by monitoring the multiple reaction monitoring Q1 300.4 m/z Q3 270.3 m/z and eluted from the HPLC column just after d18:0, identical to authentic 3-KDS standards (Matreya). The 4-hydroxy-3KDS was detected by the same multiple reaction monitoring as t18:1 but elutes as a peak just after t18:0. No standard is available for 4-hydroxy-3-KDS, but the keto chemistry of the peak was confirmed by reducing it to t18:0 through treatment with sodium borohydride.

Suberin Analysis of Wild-Type and Mutant *Arabidopsis*

Suberin was analyzed both chemically and by TEM. Root suberin monomer composition of 4-week-old plants was analyzed according to Bonaventure et al. (2004) with slight modifications described by Lü et al. (2009). Briefly, root tissue was ground, delipidated, and dried. Dried material was depolymerized in 6 mL of 3 N methanolic hydrochloride (Supelco) and 0.45 mL (7%, v/v) methyl acetate (Sigma-Aldrich) at 60°C for 16 h. Methyl heptadecanoate was used as an internal standard. Reactions were allowed to cool to room temperature and the reaction terminated by the addition of 6 mL of saturated, aqueous NaCl followed by two extractions (10 mL) with distilled dichloromethane to remove methyl ester monomers. After washing the organic phase three times with 0.9% (w/v) aqueous NaCl, dichloromethane extracts were dried with 2,2-dimethoxypropane (Sigma-Aldrich) and dried under nitrogen gas. Monomers were derivatized in pyridine and BSTFA (1:1, v/v) for 15 min at 100°C. Excess pyridine:BSTFA was evaporated under nitrogen gas, and the sample dissolved in heptane:toluene (1:1, v/v) prior to analysis with a Hewlett-Packard 5890 series II gas chromatograph. The casparin band of roots of 6-week-old plants was viewed by TEM as reported by Lü et al. (2009).

qRT-PCR

Total RNA isolation was conducted as described earlier (Chen et al., 2006). The primers used for transcript quantification of *TSC10A* and *TSC10B* are shown in Supplemental Table 2 online. Four reactions were done per biological sample, and three independent replicate samples per genotype were used to evaluate the transcript abundance of *TSC10A* and *TSC10B*. Data were analyzed using the SDS software (Applied Biosystems version 1.0), following the method of Livak and Schmittgen (2001). Cycle time (CT) values were determined based on efficiency of amplification. The mean CT values were normalized against the corresponding *UBQ10* gene (At4g05320) and CT values calculated as (CT *TSC10* − CT *UBQ10*). The expression of *TSC10A* and *TSC10B* was calculated using the $2^{\wedge(\Delta CT)}$ method. The final error was estimated by evaluating the $2^{\wedge(\Delta CT)}$ term using $2^{\wedge(\Delta CT)}$ plus SD and $2^{\wedge(\Delta CT)}$ minus the SD (Livak and Schmittgen, 2001).

Statistical Methods

Single-factor mixed effect model ANOVAs were calculated comparing a wild-type gene response to mutant gene response for data shown in Tables 1 and 2 and Figure 12. A Levene's homogeneity of variance test was first performed to check if data transformation was necessary at $P \leq 0.05$ before the ANOVAs were calculated. If a data transformation was found to stabilize the variance, all further analyses were performed on the transformed data, even though results are presented in the untransformed form for ease of interpretation. The F-test P values were corrected for the multiple tests using a Benjamini-Hochberg multiple testing correction. If a significant corrected F-test P value was obtained at $P \leq 0.05$ from an ANOVA, then differences of least squares means was used as a multiple comparison procedure to compare the wild-type gene response to that of the mutants. To account for the effect of the independent alleles for each gene, we imposed an additional filter that required that each independent line was significantly different from the wild type ($P \leq 0.05$) in the mixed effect model analysis.

Accession Numbers

Sequence data from this article can be found in the GenBank/EMBL data libraries under the following accession numbers: TSC10A (At3g06060), NM_111481; TSC10B (At5g19200), NM_121925; UBQ10 (At4g05320), AY139999; and IRT1 (At4g19690), NM_118089.

Supplemental Data

The following materials are available in the online version of this article.

Supplemental Figure 1. The Effect of Sucrose on Root Growth of *tsc10a*.

Supplemental Figure 2. Developmental Changes in *tsc10a*.

Supplemental Figure 3. Flowering and Hypocotyl Elongation Phenotypes in *tsc10a*.

Supplemental Figure 4. Segregation of the Leaf Ionomic Phenotype in 5-Week-Old F2 Plants from a L*er*-0 × *tsc10a-1* Outcross.

Supplemental Figure 5. Map-Based Cloning of *tsc10a-1*.

Supplemental Figure 6. Relationship between *Arabidopsis* TSC10A and Its Various Homologs.

Supplemental Figure 7. Wilting Resistance of *tsc10a*.

Supplemental Table 1. Predicted Transmembrane Domains in the Yeast, *Arabidopsis*, and Human 3-KDS Reductases.

Supplemental Table 2. Primers Used for PCR Amplification.

ACKNOWLEDGMENTS

This work was supported by grants from the U.S. National Science Foundation Arabidopsis 2010 Program to D.E.S. (IOB 0419695) and a collaborative grant to T.M.D. (MCB-0313466) and E.B.C. and J.G.J. (MCB-0312559), the U.S. National Science Foundation to E.B.C. (MCB-0844312), and the U.S. National Institutes of Health, National Institute of Neurological Disorders and Stroke to T.M.D. (NS47717). We thank Jonathan Napier, Frédéric Beaudoin, and Daniel Lynch for helpful discussions and Deb Palmquist for valuable assistance with the statistical analyses.

Received August 26, 2010; revised January 19, 2011; accepted February 14, 2011; published March 18, 2011.

REFERENCES

Baxter, I., Hosmani, P.S., Rus, A., Lahner, B., Borevitz, J.O., Muthukumar, B., Mickelbart, M.V., Schreiber, L., Franke, R.B., and Salt, D.E. (2009). Root suberin forms an extracellular barrier that affects water relations and mineral nutrition in Arabidopsis. PLoS Genet. **5:** e1000492.

Baxter, I., Muthukumar, B., Park, H.C., Buchner, P., Lahner, B., Danku, J., Zhao, K., Lee, J., Hawkesford, M.J., Guerinot, M.L., and Salt, D.E. (2008a). Variation in molybdenum content across broadly distributed populations of *Arabidopsis thaliana* is controlled by a mitochondrial molybdenum transporter (MOT1). PLoS Genet. **4:** e1000004.

Baxter, I., Ouzzani, M., Orcun, S., Kennedy, B., Jandhyala, S.S., and Salt, D.E. (2007). Purdue ionomics information management system. An integrated functional genomics platform. Plant Physiol. **143:** 600–611.

Baxter, I.R., Vitek, O., Lahner, B., Muthukumar, B., Borghi, M., Morrissey, J., Guerinot, M.L., and Salt, D.E. (2008b). The leaf ionome as a multivariable system to detect a plant's physiological status. Proc. Natl. Acad. Sci. USA **105:** 12081–12086.

Beeler, T., Bacikova, D., Gable, K., Hopkins, L., Johnson, C., Slife, H., and Dunn, T. (1998). The *Saccharomyces cerevisiae* TSC10/YBR265w gene encoding 3-ketosphinganine reductase is identified in a screen for temperature-sensitive suppressors of the Ca2+-sensitive csg2Delta mutant. J. Biol. Chem. **273:** 30688–30694.

Beisson, F., Li, Y.H., Bonaventure, G., Pollard, M., and Ohlrogge, J.B. (2007). The acyltransferase GPAT5 is required for the synthesis of suberin in seed coat and root of *Arabidopsis*. Plant Cell **19:** 351–368.

Bonaventure, G., Beisson, F., Ohlrogge, J., and Pollard, M. (2004). Analysis of the aliphatic monomer composition of polyesters associated with Arabidopsis epidermis: Occurrence of octadeca-cis-6, cis-9-diene-1,18-dioate as the major component. Plant J. **40:** 920–930.

Borevitz, J.O., Liang, D., Plouffe, D., Chang, H.S., Zhu, T., Weigel, D., Berry, C.C., Winzeler, E., and Chory, J. (2003). Large-scale identification of single-feature polymorphisms in complex genomes. Genome Res. **13:** 513–523.

Borner, G.H., Sherrier, D.J., Weimar, T., Michaelson, L.V., Hawkins, N.D., Macaskill, A., Napier, J.A., Beale, M.H., Lilley, K.S., and Dupree, P. (2005). Analysis of detergent-resistant membranes in Arabidopsis. Evidence for plasma membrane lipid rafts. Plant Physiol. **137:** 104–116.

Broadley, M.R., Bowen, H.C., Cotterill, H.L., Hammond, J.P., Meacham, M.C., Mead, A., and White, P.J. (2004). Phylogenetic variation in the shoot mineral concentration of angiosperms. J. Exp. Bot. **55:** 321–336.

Broadley, M.R., Hammond, J.P., White, P.J., and Salt, D.E. (2010). An efficient procedure for normalizing ionomics data for *Arabidopsis thaliana.* New Phytol. **186:** 270–274.

Buescher, E., et al. (2010). Natural genetic variation in selected populations of *Arabidopsis thaliana* is associated with ionomic differences. PLoS ONE **5:** e11081.

Chen, M., Han, G., Dietrich, C.R., Dunn, T.M., and Cahoon, E.B. (2006). The essential nature of sphingolipids in plants as revealed by the functional identification and characterization of the *Arabidopsis* LCB1 subunit of serine palmitoyltransferase. Plant Cell **18:** 3576–3593.

Chen, Y.F., Wang, Y., and Wu, W.H. (2008). Membrane transporters for nitrogen, phosphate and potassium uptake in plants. J. Integr. Plant Biol. **50:** 835–848.

Clough, S.J., and Bent, A.F. (1998). Floral dip: a simplified method for Agrobacterium-mediated transformation of *Arabidopsis thaliana.* Plant J. **16:** 735–743.

Connolly, E.L., Fett, J.P., and Guerinot, M.L. (2002). Expression of the IRT1 metal transporter is controlled by metals at the levels of transcript and protein accumulation. Plant Cell **14:** 1347–1357.

Coursol, S., Fan, L.M., Le Stunff, H., Spiegel, S., Gilroy, S., and Assmann, S.M. (2003). Sphingolipid signalling in Arabidopsis guard cells involves heterotrimeric G proteins. Nature **423:** 651–654.

Coursol, S., Le Stunff, H., Lynch, D.V., Gilroy, S., Assmann, S.M., and Spiegel, S. (2005). Arabidopsis sphingosine kinase and the effects of phytosphingosine-1-phosphate on stomatal aperture. Plant Physiol. **137:** 724–737.

Curtis, M.D., and Grossniklaus, U. (2003). A gateway cloning vector set for high-throughput functional analysis of genes in planta. Plant Physiol. **133:** 462–469.

Davin, L.B., and Lewis, N.G. (2000). Dirigent proteins and dirigent sites explain the mystery of specificity of radical precursor coupling in lignan and lignin biosynthesis. Plant Physiol. **123:** 453–462.

Delhaize, E. (1996). A metal-accumulator mutant of *Arabidopsis thaliana*. Plant Physiol. **111:** 849–855.

Dietrich, C.R., Han, G., Chen, M., Berg, R.H., Dunn, T.M., and Cahoon, E.B. (2008). Loss-of-function mutations and inducible RNAi suppression of Arabidopsis LCB2 genes reveal the critical role of sphingolipids in gametophytic and sporophytic cell viability. Plant J. **54:** 284–298.

Domergue, F., Vishwanath, S.J., Joubès, J., Ono, J., Lee, J.A., Bourdon, M., Alhattab, R., Lowe, C., Pascal, S., Lessire, R., and Rowland, O. (2010). Three Arabidopsis fatty acyl-coenzyme A reductases, FAR1, FAR4, and FAR5, generate primary fatty alcohols associated with suberin deposition. Plant Physiol. **153:** 1539–1554.

Dunn, T.M., Gable, K., Monaghan, E., and Bacikova, D. (2000). Selection of yeast mutants in sphingolipid metabolism. Methods Enzymol. **312:** 317–330.

Durrett, T.P., Gassmann, W., and Rogers, E.E. (2007). The FRD3-mediated efflux of citrate into the root vasculature is necessary for efficient iron translocation. Plant Physiol. **144:** 197–205.

Franke, R., Höfer, R., Briesen, I., Emsermann, M., Efremova, N., Yephremov, A., and Schreiber, L. (2009). The DAISY gene from Arabidopsis encodes a fatty acid elongase condensing enzyme involved in the biosynthesis of aliphatic suberin in roots and the chalaza-micropyle region of seeds. Plant J. **57:** 80–95.

Gupta, S.D., Gable, K., Han, G., Borovitskaya, A., Selby, L., Dunn, T.M., and Harmon, J.M. (2009). Tsc10p and FVT1: Topologically distinct short-chain reductases required for long-chain base synthesis in yeast and mammals. J. Lipid Res. **50:** 1630–1640.

Gustin, J.L., Loureiro, M.E., Kim, D., Na, G., Tikhonova, M., and Salt, D.E. (2009). MTP1-dependent Zn sequestration into shoot vacuoles suggests dual roles in Zn tolerance and accumulation in Zn-hyperaccumulating plants. Plant J. **57:** 1116–1127.

Han, G., Gable, K., Yan, L., Natarajan, M., Krishnamurthy, J., Gupta, S.D., Borovitskaya, A., Harmon, J.M., and Dunn, T.M. (2004). The topology of the Lcb1p subunit of yeast serine palmitoyltransferase. J. Biol. Chem. **279:** 53707–53716.

Hayashi, S., Ishii, T., Matsunaga, T., Tominaga, R., Kuromori, T., Wada, T., Shinozaki, K., and Hirayama, T. (2008). The glycerophosphoryl diester phosphodiesterase-like proteins SHV3 and its homologs play important roles in cell wall organization. Plant Cell Physiol. **49:** 1522–1535.

Hazen, S.P., Borevitz, J.O., Harmon, F.G., Pruneda-Paz, J.L., Schultz, T.F., Yanovsky, M.J., Liljegren, S.J., Ecker, J.R., and Kay, S.A. (2005). Rapid array mapping of circadian clock and developmental mutations in Arabidopsis. Plant Physiol. **138:** 990–997.

Hodges, E., Xuan, Z., Balija, V., Kramer, M., Molla, M.N., Smith, S.W., Middle, C.M., Rodesch, M.J., Albert, T.J., Hannon, G.J., and McCombie, W.R. (2007). Genome-wide in situ exon capture for selective resequencing. Nat. Genet. **39:** 1522–1527.

Höfer, R., Briesen, I., Beck, M., Pinot, F., Schreiber, L., and Franke, R. (2008). The Arabidopsis cytochrome P450 CYP86A1 encodes a fatty acid omega-hydroxylase involved in suberin monomer biosynthesis. J. Exp. Bot. **59:** 2347–2360.

Hwang, I., and Sheen, J. (2001). Two-component circuitry in Arabidopsis cytokinin signal transduction. Nature **413:** 383–389.

Kallberg, Y., and Persson, B. (2006). Prediction of coenzyme specificity in dehydrogenases/reductases. A hidden Markov model-based method and its application on complete genomes. FEBS J. **273:** 1177–1184.

Kavanagh, K.L., Jörnvall, H., Persson, B., and Oppermann, U. (2008). Medium- and short-chain dehydrogenase/reductase gene and protein families: The SDR superfamily: functional and structural diversity within a family of metabolic and regulatory enzymes. Cell. Mol. Life Sci. **65:** 3895–3906.

Kerkeb, L., Mukherjee, I., Chatterjee, I., Lahner, B., Salt, D.E., and Connolly, E.L. (2008). Iron-induced turnover of the Arabidopsis IRON-REGULATED TRANSPORTER1 metal transporter requires lysine residues. Plant Physiol. **146:** 1964–1973.

Kohlwein, S.D., Eder, S., Oh, C.S., Martin, C.E., Gable, K., Bacikova, D., and Dunn, T. (2001). Tsc13p is required for fatty acid elongation and localizes to a novel structure at the nuclear-vacuolar interface in *Saccharomyces cerevisiae*. Mol. Cell. Biol. **21:** 109–125.

Lahner, B., Gong, J., Mahmoudian, M., Smith, E.L., Abid, K.B., Rogers, E.E., Guerinot, M.L., Harper, J.F., Ward, J.M., McIntyre, L., Schroeder, J.I., and Salt, D.E. (2003). Genomic scale profiling of nutrient and trace elements in *Arabidopsis thaliana*. Nat. Biotechnol. **21:** 215–221.

Li, Y., Beisson, F., Koo, A.J., Molina, I., Pollard, M., and Ohlrogge, J. (2007). Identification of acyltransferases required for cutin biosynthesis and production of cutin with suberin-like monomers. Proc. Natl. Acad. Sci. USA **104:** 18339–18344.

Liang, H., Yao, N., Song, J.T., Luo, S., Lu, H., and Greenberg, J.T. (2003). Ceramides modulate programmed cell death in plants. Genes Dev. **17:** 2636–2641.

Livak, K.J., and Schmittgen, T.D. (2001). Analysis of relative gene expression data using real-time quantitative PCR and the 2(-Delta Delta C(T)) Method. Methods **25:** 402–408.

Lü, S., Song, T., Kosma, D.K., Parsons, E.P., Rowland, O., and Jenks, M.A. (2009). Arabidopsis CER8 encodes LONG-CHAIN ACYL-COA SYNTHETASE 1 (LACS1) that has overlapping functions with LACS2 in plant wax and cutin synthesis. Plant J. **59:** 553–564.

Lynch, D.V., and Dunn, T.M. (2004). An introduction to plant sphingolipids and a review of recent advances in understanding their metabolism and function. New Phytol. **161:** 677–702.

Markham, J.E., and Jaworski, J.G. (2007). Rapid measurement of sphingolipids from *Arabidopsis thaliana* by reversed-phase high-performance liquid chromatography coupled to electrospray ionization tandem mass spectrometry. Rapid Commun. Mass Spectrom. **21:** 1304–1314.

Markham, J.E., Li, J., Cahoon, E.B., and Jaworski, J.G. (2006). Separation and identification of major plant sphingolipid classes from leaves. J. Biol. Chem. **281:** 22684–22694.

Maurel, C., Santoni, V., Luu, D.T., Wudick, M.M., and Verdoucq, L. (2009). The cellular dynamics of plant aquaporin expression and functions. Curr. Opin. Plant Biol. **12:** 690–698.

Michelmore, R.W., Paran, I., and Kesseli, R.V. (1991). Identification of markers linked to disease-resistance genes by bulked segregant analysis: A rapid method to detect markers in specific genomic regions by using segregating populations. Proc. Natl. Acad. Sci. USA **88:** 9828–9832.

Mikosch, M., and Homann, U. (2009). How do ER export motifs work on ion channel trafficking? Curr. Opin. Plant Biol. **12:** 685–689.

Mongrand, S., Morel, J., Laroche, J., Claverol, S., Carde, J.P., Hartmann, M.A., Bonneu, M., Simon-Plas, F., Lessire, R., and Bessoule, J.J. (2004). Lipid rafts in higher plant cells: purification and characterization of Triton X-100-insoluble microdomains from tobacco plasma membrane. J. Biol. Chem. **279:** 36277–36286.

Morales, P.R., Dillehay, D.L., Moody, S.J., Pallas, D.C., Pruett, S., Allgood, J.C., Symolon, H., and Merrill, A.H., Jr. (2007). Safingol toxicology after oral administration to TRAMP mice: demonstration of safingol uptake and metabolism by N-acylation and N-methylation. Drug Chem. Toxicol. **30:** 197–216.

Morel, J., Claverol, S., Mongrand, S., Furt, F., Fromentin, J., Bessoule, J.J., Blein, J.P., and Simon-Plas, F. (2006). Proteomics of plant detergent-resistant membranes. Mol. Cell. Proteomics **5:** 1396–1411.

Morrissey, J., and Guerinot, M.L. (2009). Iron uptake and transport in plants: The good, the bad, and the ionome. Chem. Rev. **109:** 4553–4567.

Nakajima, K., Hashimoto, T., and Yamada, Y. (1994). Opposite stereospecificity of two tropinone reductases is conferred by the substrate-binding sites. J. Biol. Chem. **269:** 11695–11698.

Nawrath, C. (2002). The biopolymers cutin and suberin. The Arabidopsis Book **1:** e0021, doi/10.1199/tab.0021.

Nelson, B.K., Cai, X., and Nebenführ, A. (2007). A multicolored set of in vivo organelle markers for co-localization studies in Arabidopsis and other plants. Plant J. **51:** 1126–1136.

Ng, C., Carr, K., McAinsh, M.R., Powell, B., and Hetherington, A.M. (2001). Drought-induced guard cell signal transduction involves shpingosine-1-phosphate. Nature **410:** 596–599.

Nublat, A., Desplans, J., Casse, F., and Berthomieu, P. (2001). *sas1*,

an Arabidopsis mutant overaccumulating sodium in the shoot, shows deficiency in the control of the root radial transport of sodium. Plant Cell **13:** 125–137.

Panikashvili, D., Shi, J.X., Bocobza, S., Franke, R.B., Schreiber, L., and Aharoni, A. (2010). The Arabidopsis DSO/ABCG11 transporter affects cutin metabolism in reproductive organs and suberin in roots. Mol. Plant **3:** 563–575.

Paul, S., Gable, K., Beaudoin, F., Cahoon, E., Jaworski, J., Napier, J.A., and Dunn, T.M. (2006). Members of the Arabidopsis FAE1-like 3-ketoacyl-CoA synthase gene family substitute for the Elop proteins of *Saccharomyces cerevisiae*. J. Biol. Chem. **281:** 9018–9029.

Rogers, E.E., and Guerinot, M.L. (2002). FRD3, a member of the multidrug and toxin efflux family, controls iron deficiency responses in Arabidopsis. Plant Cell **14:** 1787–1799.

Rubio, F., Nieves-Cordones, M., Alemán, F., and Martínez, V. (2008). Relative contribution of AtHAK5 and AtAKT1 to K^+ uptake in the high-affinity range of concentrations. Physiol. Plant. **134:** 598–608.

Rus, A., Baxter, I., Muthukumar, B., Gustin, J., Lahner, B., Yakubova, E., and Salt, D.E. (2006). Natural variants of AtHKT1 enhance Na^+ accumulation in two wild populations of Arabidopsis. PLoS Genet. **2:** e210.

Salt, D.E., Baxter, I., and Lahner, B. (2008). Ionomics and the study of the plant ionome. Annu. Rev. Plant Biol. **59:** 709–733.

Schneeberger, K., Ossowski, S., Lanz, C., Juul, T., Petersen, A.H., Nielsen, K.L., Jørgensen, J.E., Weigel, D., and Andersen, S.U. (2009). SHOREmap: simultaneous mapping and mutation identification by deep sequencing. Nat. Methods **6:** 550–551.

Sedbrook, J.C., Carroll, K.L., Hung, K.F., Masson, P.H., and Somerville, C.R. (2002). The Arabidopsis SKU5 gene encodes an extracellular glycosyl phosphatidylinositol-anchored glycoprotein involved in directional root growth. Plant Cell **14:** 1635–1648.

Sherman, F., Fink, G.R., and Hicks, J.B. (1986). Methods in Yeast Genetics. (Cold Spring Harbor, NY: Cold Spring Harbor Laboratory Press).

Shi, L., Bielawski, J., Mu, J., Dong, H., Teng, C., Zhang, J., Yang, X., Tomishige, N., Hanada, K., Hannun, Y.A., and Zuo, J. (2007). Involvement of sphingoid bases in mediating reactive oxygen intermediate production and programmed cell death in Arabidopsis. Cell Res. **17:** 1030–1040.

Spassieva, S.D., Markham, J.E., and Hille, J. (2002). The plant disease resistance gene Asc-1 prevents disruption of sphingolipid metabolism during AAL-toxin-induced programmed cell death. Plant J. **32:** 561–572.

Sperling, P., Franke, S., Lüthje, S., and Heinz, E. (2005). Are glucocerebrosides the predominant sphingolipids in plant plasma membranes? Plant Physiol. Biochem. **43:** 1031–1038.

Tamura, K., Mitsuhashi, N., Hara-Nishimura, I., and Imai, H. (2001). Characterization of an Arabidopsis cDNA encoding a subunit of serine palmitoyltransferase, the initial enzyme in sphingolipid biosynthesis. Plant Cell Physiol. **42:** 1274–1281.

Teng, C., Dong, H., Shi, L., Deng, Y., Mu, J., Zhang, J., Yang, X., and Zuo, J. (2008). Serine palmitoyltransferase, a key enzyme for de novo synthesis of sphingolipids, is essential for male gametophyte development in Arabidopsis. Plant Physiol. **146:** 1322–1332.

Tian, H., Baxter, I.R., Lahner, B., Reinders, A., Salt, D.E., and Ward, J.M. (2010). *Arabidopsis* NPCC6/NaKR1 is a phloem mobile metal binding protein necessary for phloem function and root meristem maintenance. Plant Cell **22:** 3963–3979.

Townley, H.E., McDonald, K., Jenkins, G.I., Knight, M.R., and Leaver, C.J. (2005). Ceramides induce programmed cell death in Arabidopsis cells in a calcium-dependent manner. Biol. Chem. **386:** 161–166.

Uozumi, N., Kim, E.J., Rubio, F., Yamaguchi, T., Muto, S., Tsuboi, A., Bakker, E.P., Nakamura, T., and Schroeder, J.I. (2000). The Arabidopsis HKT1 gene homolog mediates inward Na(+) currents in xenopus laevis oocytes and Na(+) uptake in *Saccharomyces cerevisiae.* Plant Physiol. **122:** 1249–1259.

Vert, G., Grotz, N., Dédaldéchamp, F., Gaymard, F., Guerinot, M.L., Briat, J.F., and Curie, C. (2002). IRT1, an Arabidopsis transporter essential for iron uptake from the soil and for plant growth. Plant Cell **14:** 1223–1233.

Wang, H., Li, J., Bostock, R.M., and Gilchrist, D.G. (1996). Apoptosis: A functional paradigm for programmed plant cell death induced by a host-selective phytotoxin and invoked during development. Plant Cell **8:** 375–391.

Wang, W., et al. (2008). An inositolphosphorylceramide synthase is involved in regulation of plant programmed cell death associated with defense in *Arabidopsis*. Plant Cell **20:** 3163–3179.

Ward, J.M., Mäser, P., and Schroeder, J.I. (2009). Plant ion channels: Gene families, physiology, and functional genomics analyses. Annu. Rev. Physiol. **71:** 59–82.

Watanabe, T., Broadley, M.R., Jansen, S., White, P.J., Takada, J., Satake, K., Takamatsu, T., Tuah, S.J., and Osaki, M. (2007). Evolutionary control of leaf element composition in plants. New Phytol. **174:** 516–523.

Yang, W., Pollard, M., Li-Beisson, Y., Beisson, F., Feig, M., and Ohlrogge, J. (2010). A distinct type of glycerol-3-phosphate acyltransferase with sn-2 preference and phosphatase activity producing 2-monoacylglycerol. Proc. Natl. Acad. Sci. USA **107:** 12040–12045.

Zimmermann, P., Hirsch-Hoffmann, M., Hennig, L., and Gruissem, W. (2004). GENEVESTIGATOR. Arabidopsis microarray database and analysis toolbox. Plant Physiol. **136:** 2621–2632.